2018

MARCH1 protects the lipid raft and tetraspanin web from MHCII proteotoxicity in dendritic cells

Jaehak Oh
University of California, San Francisco

Justin S.A. Perry
University of California, San Francisco

Heather Pua
University of California, San Francisco

Nicole Irgens-Möller
University of California, San Francisco

Satoshi Ishido
Hyogo College of Medicine 1-1

See next page for additional authors

JCB

Article

MARCH1 protects the lipid raft and tetraspanin web from MHCII proteotoxicity in dendritic cells

Jaehak Oh,[1,2] Justin S.A. Perry,[3] Heather Pua,[2,3] Nicole Irgens-Möller,[1,2] Satoshi Ishido,[5] Chyi-Song Hsieh,[4] and Jeoung-Sook Shin[1,2]

[1]Department of Microbiology and Immunology, [2]Sandler Asthma Basic Research Center, and [3]Department of Pathology, University of California, San Francisco, San Francisco, CA
[4]Department of Internal Medicine, Division of Rheumatology, Washington University School of Medicine, St. Louis, MO
[5]Department of Microbiology, Hyogo College of Medicine 1-1, Mukogawa-cho, Nishinomiya, Japan

Dendritic cells (DCs) produce major histocompatibility complex II (MHCII) in large amounts to function as professional antigen presenting cells. Paradoxically, DCs also ubiquitinate and degrade MHCII in a constitutive manner. Mice deficient in the MHCII-ubiquitinating enzyme membrane-anchored RING-CH1, or the ubiquitin-acceptor lysine of MHCII, exhibit a substantial reduction in the number of regulatory T (Treg) cells, but the underlying mechanism was unclear. Here we report that ubiquitin-dependent MHCII turnover is critical to maintain homeostasis of lipid rafts and the tetraspanin web in DCs. Lack of MHCII ubiquitination results in the accumulation of excessive quantities of MHCII in the plasma membrane, and the resulting disruption to lipid rafts and the tetraspanin web leads to significant impairment in the ability of DCs to engage and activate thymocytes for Treg cell differentiation. Thus, ubiquitin-dependent MHCII turnover represents a novel quality-control mechanism by which DCs maintain homeostasis of membrane domains that support DC's Treg cell–selecting function.

Introduction

Membrane-anchored RING-CH1 (MARCH1) is a membrane-anchored ubiquitin ligase expressed in hematopoietic cells, particularly antigen presenting cells (Matsuki et al., 2007). It is composed of an N-terminal cytoplasmic tail that possesses a catalytic RING domain, two transmembrane domains that interact with a specific substrate, and a C-terminal cytoplasmic tail. Upon recognition of substrate, MARCH1 brings a ubiquitinated E2 ubiquitin-conjugating enzyme into close proximity of its RING domain and substrate and catalyzes ubiquitin transfer from E2 to substrate. Transferred ubiquitin molecules serve as a signaling motif for endocytosis and lysosomal sorting, resulting in internalization and lysosomal degradation of the substrate (Lehner et al., 2005; Ohmura-Hoshino et al., 2006).

Several immune-associated molecules have been shown to be endocytosed and degraded in cells overexpressing MARCH1 (Bartee et al., 2004). However, major histocompatibility complex II (MHCII) and CD86 are the only molecules shown to be ubiquitinated by MARCH1 under physiological conditions (Matsuki et al., 2007; De Gassart et al., 2008; Baravalle et al., 2011). MHCII has an evolutionally conserved lysine in the cytoplasmic tail in its β-chain, and this lysine is targeted for ubiquitination (Shin et al., 2006; van Niel et al., 2006; Oh and Shin, 2015). CD86 has multiple lysines in the cytoplasmic tails, and many of these lysines can be ubiquitinated (Baravalle et al., 2011; Corcoran et al., 2011). In accordance with the role of MARCH1 in mediating ubiquitination and endocytosis of MHC II and CD86, MARCH1 ablation resulted in a marked increase in the surface expression of these two molecules in dendritic cells (DCs) in mice. Interestingly, these mice exhibited a significant reduction in the number of regulatory T (Treg) cells in the thymus (Oh et al., 2013). More interestingly, mice deficient in the cytoplasmic lysine (K) of MHCII (called "MHCII K" here) exhibited a similar deficiency in thymic Treg cells (Oh et al., 2013). Furthermore, DCs deficient in MARCH1 or MHC II K were defective at differentiating immature thymocytes to Treg cells in vitro (Oh et al., 2013). This finding suggests that MHCII ubiquitination plays an important role in DC function of selecting Treg cells. However, the underlying mechanisms have not been identified.

Treg cells are selected through a cognate interaction of $CD4^+$ thymocytes with thymic antigen-presenting cells, and the strength of this interaction is one of the key determinants for Treg cell selection (Hsieh et al., 2012; Stritesky et al., 2012; Klein et al., 2014). Low-avidity interaction does not relay sufficient signal to interacting thymocytes for expression of foxp3, the key transcription factor that guides Treg cell differentiation, whereas high-avidity interaction triggers apoptotic cell death resulting in negative selection of the interacting thymocytes.

Correspondence to Jeoung-Sook Shin: jeoung-sook.shin@ucsf.edu

Supplemental material can be found at:
http://doi.org/10.1083/jcb.201611141

The Rockefeller University Press
J. Cell Biol.
https://doi.org/10.1083/jcb.201611141

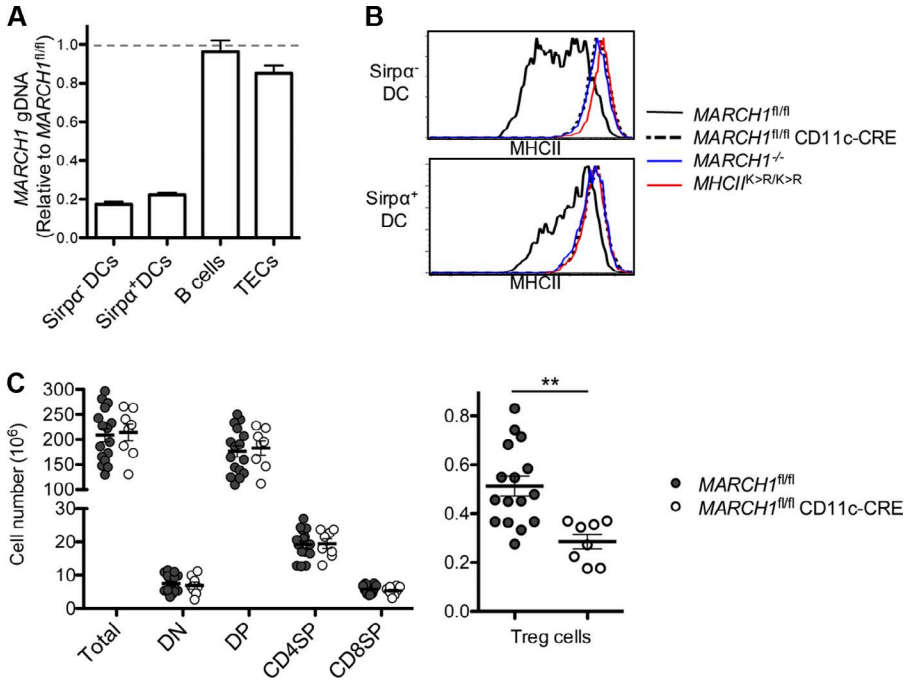

Figure 1. **DC expression of MARCH1 is important for Treg cell development in the thymus. (A)** The amount of loxp-flanked MARCH1 genomic DNA (gDNA) in Sirpα⁻ thymic DCs, Sirpα⁺ thymic DCs, thymic B cells, and thymic epithelial cells (TECs) in MARCH1$^{fl/fl}$ CD11c-CRE mice relative to MARCH1$^{fl/fl}$ mice. Each cell type was isolated by FACS as described previously (Oh et al., 2013). Data are averaged from three individual mice. **(B)** Surface expression of MHCII in Sirpα⁻ and Sirpα⁺ thymic DCs of MARCH1$^{fl/fl}$, MARCH1$^{fl/fl}$ CD11c-CRE, MARCH1$^{-/-}$, and MHCII$^{K>R/K>R}$ mice. Data represent three independent experiments. **(C)** Numbers of total, CD4⁻CD8⁻ (DN), CD4⁺CD8⁺ (DP), CD4⁺CD8⁻ (CD4SP), and CD4⁻CD8⁺ (CD8SP) thymocytes and Treg cells (CD4⁺CD8⁻Foxp3⁺CD25⁺) in MARCH1$^{fl/fl}$ and MARCH1$^{fl/fl}$ CD11c-CRE mice. Each circle represents an individual mouse. Error bars represent SEM. **, $P < 0.01$.

Only the intermediate-avidity interaction delivers a signal appropriate for Treg cell differentiation.

DCs deficient in MARCH1 or the MHCII K display peptide-loaded MHCII (pMHCII) at much larger amounts than WT DCs on the surface (Walseng et al., 2010; Oh et al., 2013). Because pMHCII is the molecule that mediates a cognate interaction of DCs with CD4⁺ thymocytes, an increase in pMHCII in DCs will increase DC avidity for antigen-specific thymocytes. The increased avidity is then likely to drive the thymocytes to apoptotic cell death while repressing differentiation into Treg cells. However, the mice deficient in MARCH1 or MHCII K did not show any increase in apoptotic cell death of CD4⁺ thymocytes or Treg cells (Oh et al., 2013). Furthermore, lowering the amount of the peptide loaded onto MHCII did not restore the development of Treg cells in MARCH1 or MHCII K–deficient mice (Oh et al., 2013). This finding suggests that the role of MARCH1 in supporting DC function of selecting Treg cells is independent of controlling surface expression of pMHCII. In this study, we have investigated the specific mechanism by which MARCH1-dependent MHCII ubiquitination supports DC selection of Treg cells.

Results

DC expression of MARCH1 is important for Treg cell development in the thymus

To determine the extent to which DCs contribute to the role of MARCH1 in promoting Treg cell development in vivo, we generated mice with loxP-flanked alleles of the RING domain of MARCH1 and bred them to CD11c-CRE transgenic mice expressing CRE recombinase under the control of the CD11c promoter (MARCH1$^{fl/fl}$ CD11c-CRE mice, Fig. S1). The loxP-flanked region of MARCH1 was efficiently and specifically deleted in DCs of MARCH1$^{fl/fl}$CD11c-CRE mice (Fig. 1 A). DCs in these mice expressed MHCII at markedly elevated levels, similar to DCs from MARCH1-deficient mice (MARCH1$^{-/-}$) or MHCII K–deficient mice (MHCII$^{K>R/K>R}$, the mice in which the ubiquitin acceptor lysine K of MHCII was replaced with arginine [R]; Fig. 1 B). MARCH1$^{fl/fl}$CD11c-CRE mice had a normal number of total, CD4⁻CD8⁻, CD4⁺CD8⁺, CD4⁺CD8⁻, and CD4⁻CD8⁺ thymocytes, but the number of Treg cells was reduced by approximately half (Fig. 1 C), similarly to what has been observed in MARCH1$^{-/-}$ mice and MHC II$^{K>R/K>R}$ mice (Oh et al., 2013). Thus, the role of MARCH1 in promoting Treg cell development is critically dependent on MARCH1 expressed in DCs.

MARCH1-mediated MHCII ubiquitination is required for DCs to effectively engage and activate thymocytes

We have previously shown that DCs deficient in MARCH1 were poor at differentiating immature thymocytes into Treg cells in vitro. To determine how MARCH1 deficiency impairs DC function of developing Treg cells, we examined whether MARCH1 is important for DCs to stably engage thymocytes and provide sufficient stimulatory signal for activation. DCs were isolated from thymi of MARCH1-deficient mice, loaded with ovalbumin, and co-cultured with CD4⁺ thymocytes isolated from the mice expressing ovalbumin-specific T cell receptor (TCR; OT-II mice). 3 h later, the number of DCs that formed stable conjugate with thymocytes was determined by flow cytometry. We found that MARCH1-deficient DCs were engaged by thymocytes to a lower frequency than WT DCs (Fig. 2, A and B). 24 h later, we also determined the expression of CD69 and CD25 in thymocytes, specific indicators of thymocyte activation involving early and late TCR signaling, respectively. We found that the thymocytes cultured with MARCH1-deficient DCs expressed CD69 to a significantly lower frequency than those cultured with WT DCs (Fig. 2, C and D). The thymocytes that had been cultured with MARCH1-deficient DCs and expressed CD69 were found to express lower levels of CD25 than those cultured with WT DCs. (Fig. 2, C and E). These findings indicate that MARCH1 is required for DCs to stably engage thymocytes and provide them with strong and/or sustained signal for activation. It is noteworthy that MARCH1-deficient

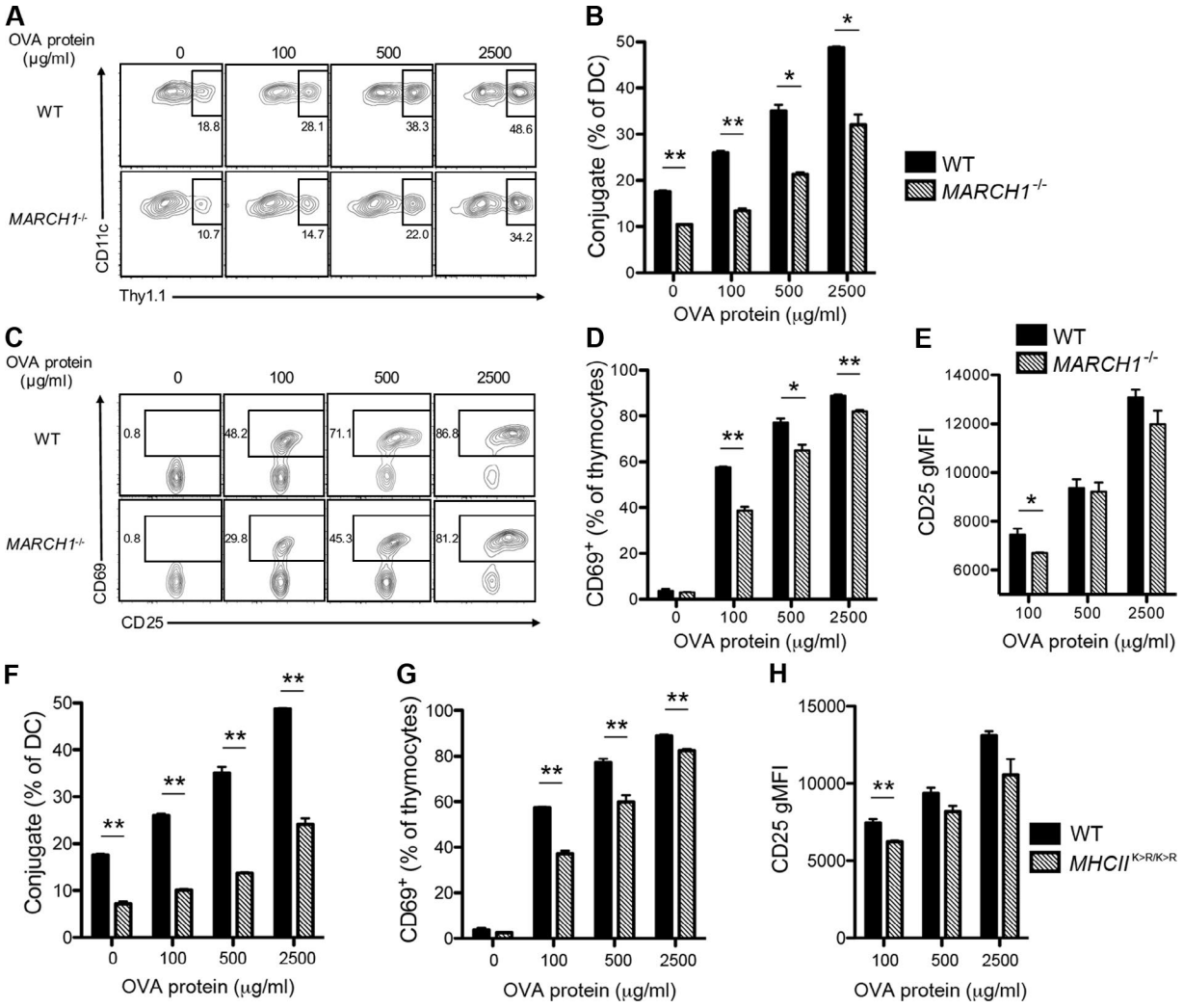

Figure 2. **MARCH1 or MHCII K–deficient DCs are incompetent to stably engage and sufficiently activate CD4+ thymocytes. (A–E)** DCs were isolated from WT or MARCH1$^{-/-}$ mouse thymi and co-cultured with CD4$^+$CD8$^-$ thymocytes isolated from OT-II mice in the presence of increasing concentrations of ovalbumin. After 3 h, the percentage of DCs that formed a stable conjugate with thymocytes was determined by flow cytometry as described in Materials and methods. The representative contour plots are shown in A, and the quantitative summary is shown in B. After 24 h, the expression of CD69 and CD25 in thymocytes was determined by flow cytometry. The representative contour plots are shown in C. The percentages of thymocytes that expressed CD69 are shown in D, and the level of CD25 expressed in the CD69$^+$ thymocytes (geometric mean fluorescence intensity [gMFI]) are shown in E. **(F–H)** DCs were isolated from WT or MHCII$^{K>R/K>R}$ mouse thymi, co-cultured with CD4$^+$CD8$^-$ thymocytes isolated from OT-II mice in the presence of increasing concentrations of ovalbumin, and examined as described in the previous section. The percentage of DCs that formed a stable conjugate with thymocytes is shown in F, the percentage of thymocytes that expressed CD69 is shown in G, and the level of CD25 expressed in CD69$^+$ thymocytes is shown in H. Data points represent two to three independent experiments with duplicate or triplicate per condition. Error bars represent SEM. *, P < 0.05; **, P < 0.01.

DCs were not much different from DCs of WT mice for the level of expression of the costimulatory molecule CD80 and the adhesion molecule ICAM1 (Fig. S2 A).

Next, we examined whether the role of MARCH1 in promoting DC engagement and activation of thymocytes depends on its activity of mediating ubiquitination of MHCII. For this examination, DCs were isolated from thymi of MHCII$^{K>R/K>R}$ mice and analyzed as described earlier. Similar to MARCH1-deficient DCs, MHCII K–deficient DCs engaged and activated thymocytes less efficiently than WT DCs (Fig. 2, F–H). MHC II K–deficient DCs were not altered for the expression of CD86, CD80, and ICAM-1 compared with WT DCs (Fig. S2 B). This finding indicates that the effect of MARCH1 in promoting DC engagement and activation of thymocytes is largely dependent on its ability to ubiquitinate MHCII.

The presence of too many MHCII molecules, not the absence of ubiquitinated MHCII, is responsible for poor engagement and activation of thymocytes by MHCII K–deficient DCs

To identify the specific mechanism by which MHCII ubiquitination supports DC engagement and activation of thymocytes, we used bone marrow–derived DCs (BMDCs), which showed a similar dependence on MHCII ubiquitination to engage and activate thymocytes (Fig. 3, B–D). We first tested whether too-high expression of MHCII or the absence of ubiquitinated MHC II is responsible for the poor engagement and activation of thymocytes by MHCII K–deficient DCs. To reduce surface MHC II levels without introducing MHCII ubiquitination, we crossed MHCII$^{K>R/K>R}$ mice to MHCII$^{-/-}$ mice and derived BMDCs from

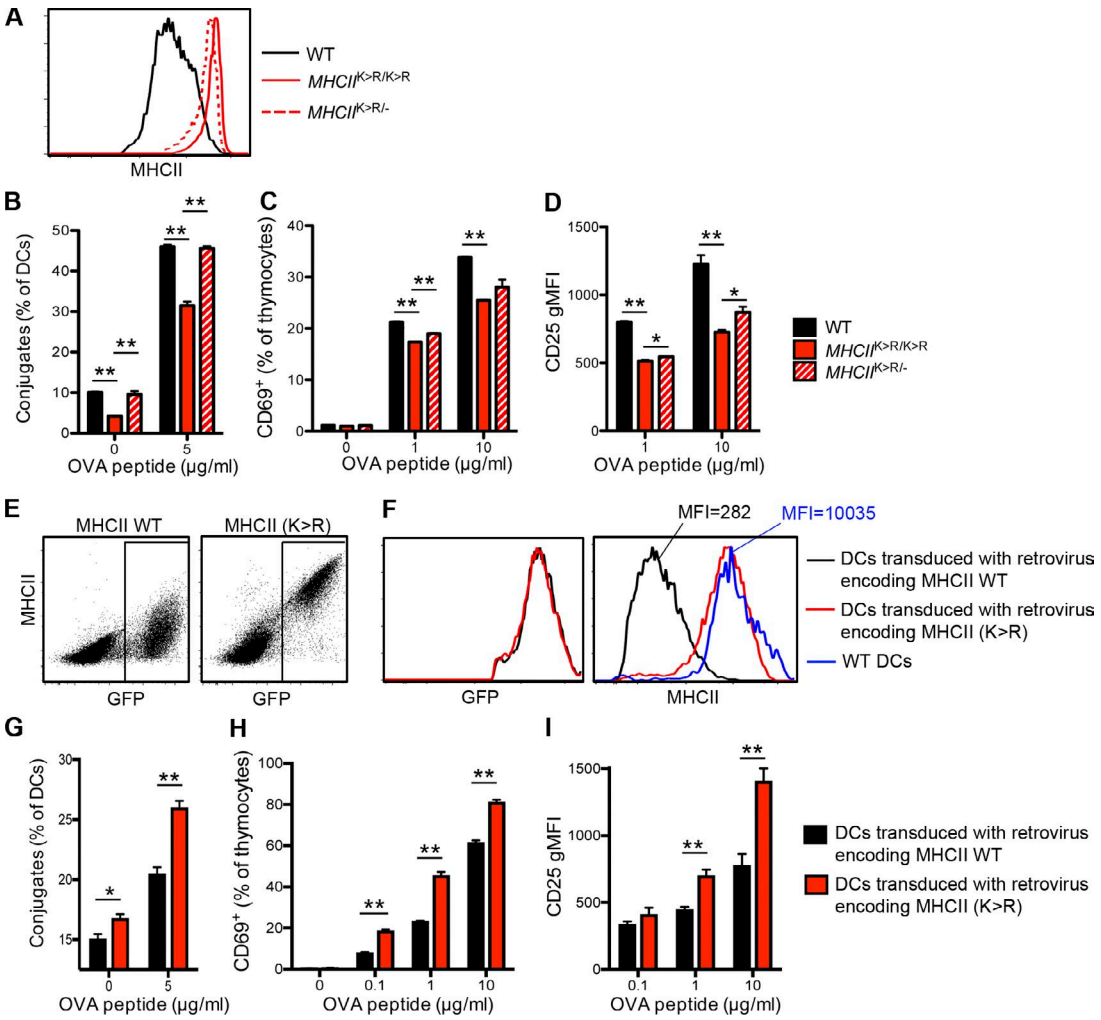

Figure 3. **The presence of too many MHCII molecules, not the absence of ubiquitinated MHCII, is responsible for poor engagement and activation of thymocytes by MHCII K-deficient DCs. (A–D)** BMDCs were derived from WT, MHCII$^{K>R/K>R}$, and MHCII$^{K>R/-}$ mice. The surface expression of MHCII is shown in A. The BMDC was cultured with CD4$^+$CD8$^-$ thymocytes isolated from OT-II mice in the presence of increasing concentrations of OVA$_{323-339}$ peptide. The percentage of DCs that formed stable conjugates with thymocytes is shown in B. The percentage of thymocytes that expressed CD69 is shown in C. The level of CD25 expressed in CD69$^+$ thymocytes is shown in D. **(E and F)** BMDCs were derived from MHCIIβ$^{-/-}$ mice and transduced with retrovirus encoding MHCIIβ WT or MHCIIβ (K>R) mutant along with cytosolic GFP. The efficiency of transduction and the expression of MHCII in transduced cells were determined by flow cytometry. The representative dot plots are shown in E (cells transduced with retrovirus encoding MHCII WT and MHCII [K>R] mutant are shown in left and right, respectively). The expression level of GFP and MHCII in transduced cells is shown in F (left and right panel, respectively). The level of MHCII expressed in DCs derived from WT mice was overlaid for comparison (blue in the right panel of F). The MFI of the MHCII stain in DCs transduced with retrovirus encoding MHCII WT and DCs derived from WT mice is indicated in F. **(G–I)** BMDCs were derived from MHCIIβ$^{-/-}$ mice and transduced with retrovirus encoding MHCIIβ WT or MHCIIβ (K>R) mutant along with cytosolic GFP. Transduced cells (GFP$^+$ cells) were isolated by FACS and cultured with CD4$^+$CD8$^-$ thymocytes isolated from OT-II mice in the presence of increasing concentrations of OVA$_{323-339}$ peptide. The percentage of DCs that formed stable conjugates with thymocytes is shown in G. The percentage of thymocytes that expressed CD69 is shown in H. The level of CD25 expressed in CD69$^+$ thymocytes is shown in I. Data represent at least three independent experiments with triplicates for each condition. Error bars represent SEM. *, P < 0.05; **, P < 0.01.

resulting MHCII$^{K>R/-}$ mice. These BMDCs expressed MHCII at slightly lower levels than BMDCs from MHCII$^{K>R/K>R}$ mice on the surface (Fig. 3 A). Interestingly, these DCs engaged thymocytes significantly better than DCs derived from MHCII$^{K>R/K>R}$ mice, suggesting that too-high MHCII, not the absence of ubiquitinated MHCII, exerted a negative impact on the ability of DCs to engage thymocytes (Fig. 3 B). DCs derived from MHC II$^{K>R/-}$ mice also activated thymocytes more effectively than DCs derived from MHCII$^{K>R/K>R}$ mice, although the degree of improvement was marginal (Fig. 3, C and D).

To further reduce surface MHCII levels in DCs, we expressed in DCs MHCII WT and MHCII (K>R) mutants using an exogenous promoter. BMDCs were cultured from MHC II$^{-/-}$ mice and transduced with the retrovirus encoding MHC II WT or MHCII (K>R) mutant (Shin et al., 2006). The retrovirus encoding MHCII WT successfully drove the expression of MHCII in DCs (Fig. 3 E), but the level was low as ∼3% of the level expressed by the endogenous promoter (Fig. 3 F). DCs transduced with the retrovirus encoding MHCII (K>R) mutant expressed much higher levels of MHCII than DCs transduced with the retrovirus encoding MHCII WT but did not reach to the level expressed by DCs derived from WT mice (Fig. 3 F). Remarkably, we found that the DCs transduced with the retrovirus encoding MHCII (K>R) mutant were superior to DCs transduced with the retrovirus encoding MHCII WT both at engaging and at activating thymocytes

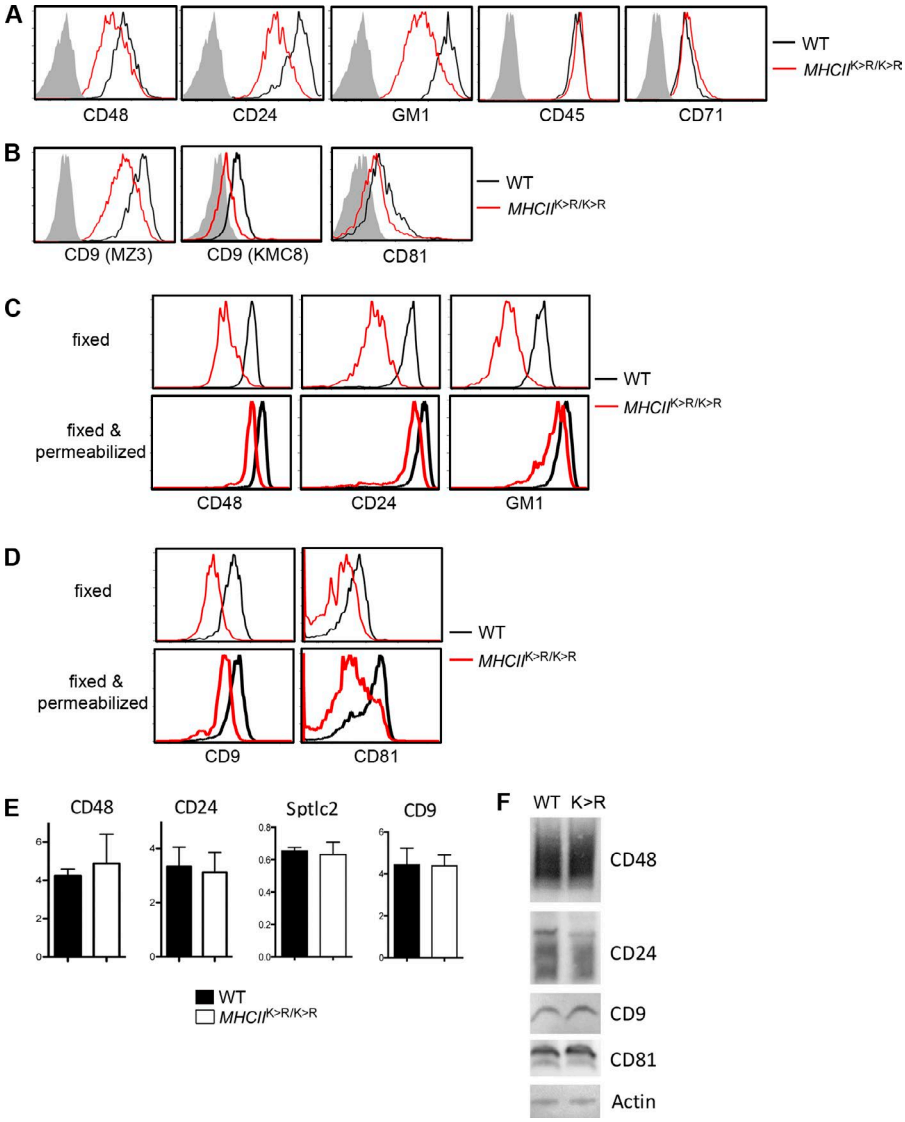

Figure 4. **MHCII K deficiency causes DCs to be poorly bound by antibodies or ligand directed to the molecules associated with the lipid raft and tetraspanin web. (A and B)** BMDCs derived from WT or MHCII$^{K>R/K>R}$ mice were stained by using monoclonal antibodies raised against indicated molecules except that CTxB was used to detect GM1. Note that two monoclonal antibodies (MZ3 and KMC8) were used for CD9. Isotype control antibodies or unstained cells (for CTxB) were used as background (gray). Sirpα^{-} DCs are shown as the representative of BMDCs. **(C and D)** BMDCs derived from WT or MHCII$^{K>R/K>R}$ mice were fixed with paraformaldehyde. Some were subsequently permeabilized and some were not before staining with antibodies or CTxB as described in A and B. Sirpα^{-} DCs are shown as the representative. **(E)** BMDCs derived from WT or MHCII$^{K>R/K>R}$ mice were lysed with TRIzol, and the amount of mRNA of indicated molecules was determined by quantitative RT-PCR. Data were normalized to mRNA of HPRT. Error bars represent SEM. **(F)** BMDCs derived from WT or MHCII$^{K>R/K>R}$ mice were run on SDS-PAGE and probed by using antibodies raised against indicated molecules. Data represent two to four independent experiments.

(Fig. 3, G–I). This finding provides definitive evidence that the failure of MHCII K–deficient DCs to effectively engage and activate thymocytes was because of the presence of too many MHCII molecules and not the absence of ubiquitinated MHCII in the cells.

MHCII K deficiency alters the lipid raft and tetraspanin web in the plasma membrane of DCs

We sought to identify the specific mechanism by which too many MHCII molecules impair DC ability to engage and activate thymocytes. MHCII is not randomly scattered in the plasma membrane of DCs but is associated with a distinct membrane domain named lipid raft, an ordered membrane structure composed of discrete species of lipids, including cholesterol, sphingolipid, and glycolipid (Anderson et al., 2000; Anderson and Roche, 2015). The lipid raft also encompasses a specific set of proteins including glycosylphosphatidylinositol (GPI)-anchored molecules (Simons and Sampaio, 2011). Although the mechanism by which MHCII associates with the lipid raft is not clearly understood, this association increases the local concentration of MHCII loaded with antigens lowering the threshold of antigen-specific T cell activation (Anderson et al., 2000). We found that MHCII in MHCII K–deficient DCs was fractionated into the light-buoyant density fractions at degrees similar to MHCII in WT DCs (Fig. S3), indicating that ubiquitination is not required for MHC II to associate with the lipid raft. However, we noticed that the absolute amount of MHCII associated with the lipid raft was markedly high in MHCII K–deficient DCs, although the amount associated with nonlipid raft was also high (Fig. S3). Because the lipid raft is an ordered structure made by tight interactions between lipids and proteins, we speculated that excessive accumulation of MHCII in the lipid raft might have altered the integrity of the structure, which in turn negatively affected the ability of MHCII K–deficient DCs to engage and activate thymocytes. Interestingly, we found that the antibodies raised against the GPI-anchored molecule CD48 or CD24 poorly bound to MHCII K–deficient DCs compared with WT DCs (Fig. 4 A). Cholera toxin B (CTxB), a specific ligand of the sphingolipid GM1, also poorly bound to MHCII K–deficient DCs (Fig. 4 A). However, the antibodies raised against the nonraft molecules CD45 and CD71 bound to MHC II K–deficient DCs similarly to WT DCs (Fig. 4 A).

In addition to the lipid raft, another membrane domain named tetraspanin web associates MHCII in DCs (Kropshofer

et al., 2002; Unternaehrer et al., 2007). This membrane domain consists of tetraspanin molecules and a limited number of partner proteins and is enriched with cholesterol and the sphingolipid ganglioside similarly to the lipid raft (Charrin et al., 2014). We found that the antibodies raised against the tetraspanin molecule CD9 or CD81 also poorly bound to MHCII K–deficient DCs compared with WT DCs (Fig. 4 B). Antibodies raised against CD63, CD37, or CD54 did not bind to either WT or MHCII K–deficient DCs possibly by little expression of these tetraspanins in the DC surface (unpublished data). These findings suggest that MHCII K deficiency induces substantial alteration in the composition or structure of the lipid raft and tetraspanin web in DC plasma membrane.

To better characterize alteration of the lipid raft and tetraspanin web in MHCII K–deficient DCs, we examined whether the alteration was restricted to the plasma membrane or also made in the intracellular compartments. First, we examined whether the aforementioned antibodies or CTxB bind more poorly to MHCII K–deficient DCs than WT DCs after fixation. As shown in Fig. 4 C. the antibodies and CTxB poorly bound to fixed MHCII (K>R) DCs compared with fixed WT DCs. Then, we permeabilized the fixed DCs and stained them with the antibodies and CTxB. Permeabilization substantially increased the binding of anti-CD48 antibody, anti-CD24 antibody, and CTxB, implicating the presence of these molecules in intracellular compartments (Fig. 4 C). Notably, we found that permeabilization markedly reduced the difference in binding of the antibodies or CTxB between MHCII K–deficient DCs and WT DCs (Fig. 4 C), suggesting that the lipid raft in the intracellular compartments of MHCII K–deficient DCs is not altered as much as that in the plasma membrane.

CD9 appeared mostly localized in the plasma membrane in DCs because permeabilization increased anti-CD9 antibody binding only to a marginal level (Fig. 4 C). The difference in binding of anti-CD9 antibody between WT and MHC II K–deficient DCs did not look much different after permeabilization. Binding of anti-CD81 antibody was substantially increased after permeabilization, implicating the presence of a substantial amount of intracellular CD81 (Fig. 4 D). The degree of binding difference between WT and MHCII K–deficient DCs also increased after permeabilization indicating that there might be substantial alteration in CD81-associating tetraspanin web in the intracellular compartments of MHCII K-deficient DCs (Fig. 4 D).

Next, we examined whether MHCII K–deficient DCs expressed lipid raft or tetraspanin molecules at lower levels than WT DCs. First, we determined the level of mRNA by quantitative RT-PCR. We did not find any significant reduction in the amount of transcript of CD48, CD24, CD9, or Sptlc2, the key enzyme in sphingolipid biosynthesis, in MHCII K–deficient DCs compared with WT DCs (Fig. 4 E). Second, we examined the protein amount by Western blot analysis. No difference was observed in the amount of CD48, CD9, or CD81, although the amount of CD24 appeared slightly lower in MHCII K–deficient DCs (Fig. 4 F). Thus, MHCII K–deficient DCs express CD48, CD9, and CD81 at levels similar to WT DCs whereas CD24 might be expressed at slightly lower levels. Collectively, we conclude that that MHCII K deficiency in DCs is accompanied by substantial changes in the conformation and stability of the molecules associated with the lipid raft and tetraspanin web in the plasma membrane.

MHCII overcrowding is responsible for the alteration of the lipid raft and tetraspanin web in MHCII K–deficient DCs

Next, we determined whether the alteration of the lipid raft and tetraspanin web in MHCII K–deficient DCs was caused by MHC II overcrowding. DCs were cultured from $MHCII^{K>R/-}$ mice and examined whether these DCs are better bound by anti-CD48, -CD24, or -CD9 antibodies and CTxB than DCs derived from $MHCII^{K>R/K>R}$ mice. We found that all of these antibodies and CTxB bound better to DCs derived from $MHCII^{K>R/-}$ mice (Fig. 5 A). We also examined binding of these antibodies and CTxB to DCs that expressed the MHCII (K>R) mutant and WT under the retroviral promoter described in Fig. 3. All the antibodies and CTxB bound to DCs that expressed MHCII WT or the MHCII (K>R) mutant at similar levels (Fig. 5 B). These findings strongly support the hypothesis MHCII overcrowding is responsible for the alteration of the lipid raft and tetraspanin web in MHCII K–deficient DCs.

To further confirm that the alteration of the lipid raft and tetraspanin web in MHCII K–deficient DCs is attributed directly to MHCII overcrowding, we ablated MHCII ubiquitination in DCs in an inducible manner. The $MARCH1^{fl/fl}$ mice described in Fig. 1 were crossed with ERT-Cre mice, which expressed estrogen receptor–Cre fusion protein under the human ubiquitin promoter. BMDCs were cultured from these mice and treated with the ligand of the estrogen receptor tamoxifen. Tamoxifen was expected to enter DCs and trigger cre-dependent recombination of the MARCH1 gene. We found that tamoxifen treatment resulted in an increase in the surface level of MHCII in as early as 24 h (Fig. 5 C). Importantly, this increase was accompanied by a reduction in the binding of anti-CD48, -CD24, or -CD9 antibodies but not CTxB (Fig. 5 C). On day 3 to 5 after tamoxifen treatment, the level of surface MHCII further increased whereas the binding of anti-CD48, -CD24, or -CD9 antibodies further decreased, and CTxB binding also decreased (Fig. 5 C). These data demonstrate a strong correlation between the degree of MHCII overcrowding and the degree of alteration of the lipid raft and tetraspanin web, further supporting that MHCII overcrowding is the direct cause of alteration in these membrane domains. In addition, this finding suggests that GPI-anchored molecules and tetraspanin molecules are more readily altered than GM1 by MHCII overcrowding.

Because MARCH1 ablation increases not only MHCII but also CD86, we tested whether CD86 accumulation may also induce similar alteration in the lipid raft and tetraspanin web. DCs derived from WT mice were transduced with the retrovirus encoding CD86 (K>R) mutant in which the cytoplasmic lysines of CD86 were replaced with arginines (Baravalle et al., 2011). We found that the cells transduced with this retrovirus expressed >50 times as many CD86 molecules as untransduced cells. However, the transduced and untransduced cells were bound by anti-CD24, -CD48, or -CD9 antibody and CTxB similarly (Fig. S4), indicating that CD86 overcrowding does not make an alteration similar to what MHCII overcrowding makes.

Lipid raft and tetraspanin web support DC engagement and activation of thymocytes

We examined whether intact lipid raft or tetraspanin web is required for DCs to stably engage and sufficiently activate thymocytes. First, we disturbed the organization of these membrane domains by using methyl β-cyclodextrin (MβCD), a

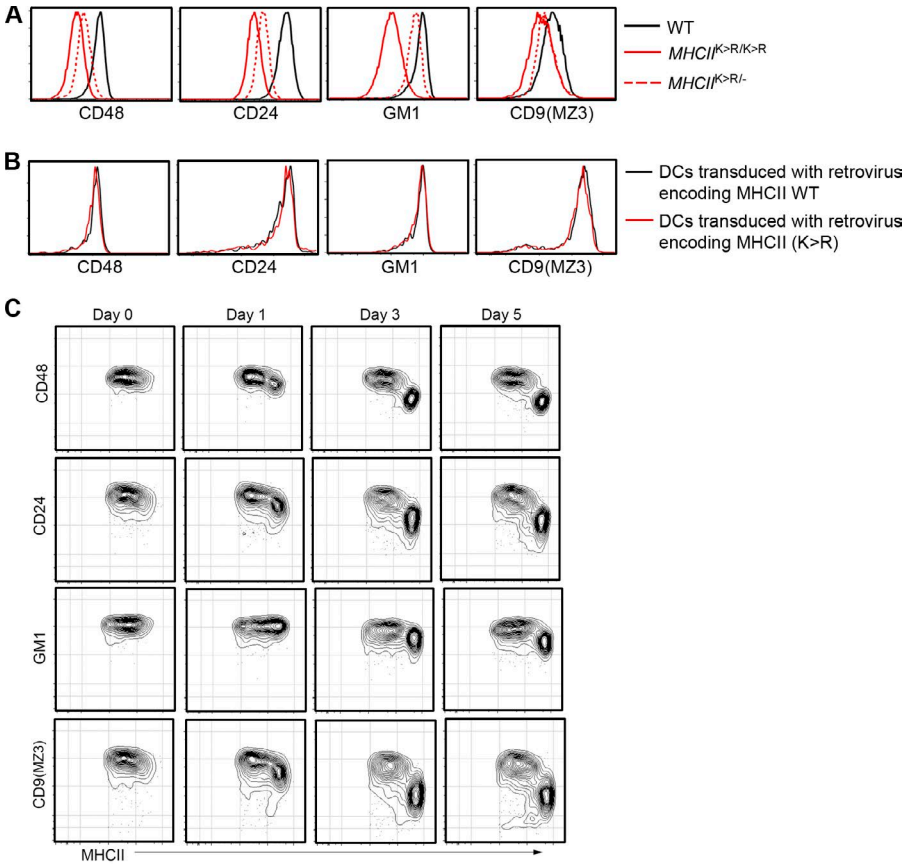

Figure 5. **MHCII overcrowding is responsible for alteration of the lipid raft and tetraspanin web in MHCII K–deficient DCs. (A)** BMDCs derived from WT, MHCII$^{K>R/K>R}$, or MHCII $^{K>R/-}$ mice were stained by using monoclonal antibodies raised against indicated molecules except that CTxB was used to detect GM1. Sirpα^{-} DCs are shown as the representative. **(B)** BMDCs derived from MHCIIβ$^{-/-}$ mice and subsequently transduced with retrovirus encoding MHCII WT or MHCII (K>R) mutant were treated and analyzed as described in A. Sirpα^{-} DCs are shown as the representative. **(C)** BMDCs cultured from MARCH1$^{fl/fl}$ERT-Cre mice were treated with tamoxifen. On days 0, 1, 3, and 5 posttreatment, cells were stained with CTxB (to detect GM1) or antibodies raised against CD48, CD24, CD9, or MHCII. Sirpα^{-} DCs are shown as the representative. Data represent two to four independent experiments.

cholesterol-chelating agent (Charrin et al., 2003). MβCD treatment diminished DC binding by anti-CD48, -CD24, or -CD9 antibodies, and CTxB (Fig. 6 A), similarly to what MHCII K deficiency did. MβCD treatment also impaired DC ability to engage and activate thymocytes (Fig. 6, B–D). Next, we treated BMDCs with myriocin, a potent and specific inhibitor of sptlc2 (Hanada, 2003). Myriocin did not impair DC binding by anti-CD48 or -CD24 antibodies although it modestly impaired binding by CTxB and anti-CD9 or -CD81 antibodies (Fig. 6 E). Myriocin treatment significantly reduced the efficiency of DCs to engage and activate thymocytes (Fig. 6, F–H). Notably however, myriocin treatment markedly reduced the surface expression of MHCII in DCs (unpublished data). Because surface MHCII makes a direct impact on the efficiency of DC activation of antigen-specific thymocytes, it is unclear whether the reduced engagement and activation of thymocytes by myriocin-treated DCs is the result of the perturbation of the lipid raft or tetraspanin web or the reduced surface expression of MHCII.

Then, we examined whether any specific molecules associated with the lipid raft or tetraspanin web are important for DCs to stably engage and sufficiently activate thymocytes. To this end, we pretreated DCs with anti-CD48, -CD24, -CD9, or -CD81 antibodies before culturing with OT-II thymocytes. We found that all of the antibodies appreciably reduced DC engagement with thymocytes compared with the control antibody (anti-TNP), although the statistically significant difference was reached only by anti-CD48 antibody and the KMC8 anti-CD9 antibody. (Fig. 6 I). These two antibodies also reduced DC engagement and activation of thymocytes at significant levels (Fig. 6, J and K). This finding implicates the role of CD48 and CD9 in DC engagement and activation of thymocytes and suggests that alteration of these two molecules may be the primary cause for diminished engagement and activation of thymocytes by MHCII K–deficient DCs.

Sphingomyelin supplementation lessens the alteration of the lipid raft and tetraspanin web in MHCII K–deficient DCs and improves the ability of the DCs to engage and activate thymocytes and drive Treg cell differentiation

We sought to determine the specific mechanism by which MHC II overcrowding alters the lipid raft or tetraspanin web and determine whether this alteration is responsible for poor engagement and activation of thymocytes by MHCII K–deficient DCs. It has been suggested that MHCII binds cholesterol and sphingolipid through its transmembrane domain (Roy et al., 2013; Björkholm et al., 2014). We postulated that cholesterol and sphingolipid in the lipid raft and tetraspanin web may be sequestered by MHCII because MHCII accumulates in these membrane domains. This sequestration would make other molecules associated with the lipid raft or tetraspanin web deprived of cholesterol or sphingolipid, resulting in alteration in the conformation or stability of the molecules. To test this hypothesis, we supplemented MHC II K–deficient DC culture with cholesterol or sphingomyelin and examined whether this supplementation makes the DCs better bound by anti-CD48, -CD24, -CD9, or -CD81 antibodies or CTxB. We found that sphingomyelin significantly improved DC binding by all these reagents (Fig. 7 A) although cholesterol did not (not depicted). Importantly, sphingomyelin also significantly improved the ability of MHCII K–deficient DCs to engage and activate thymocytes (Fig. 7, B–D). Then, we examined whether sphingomyelin treatment also improves

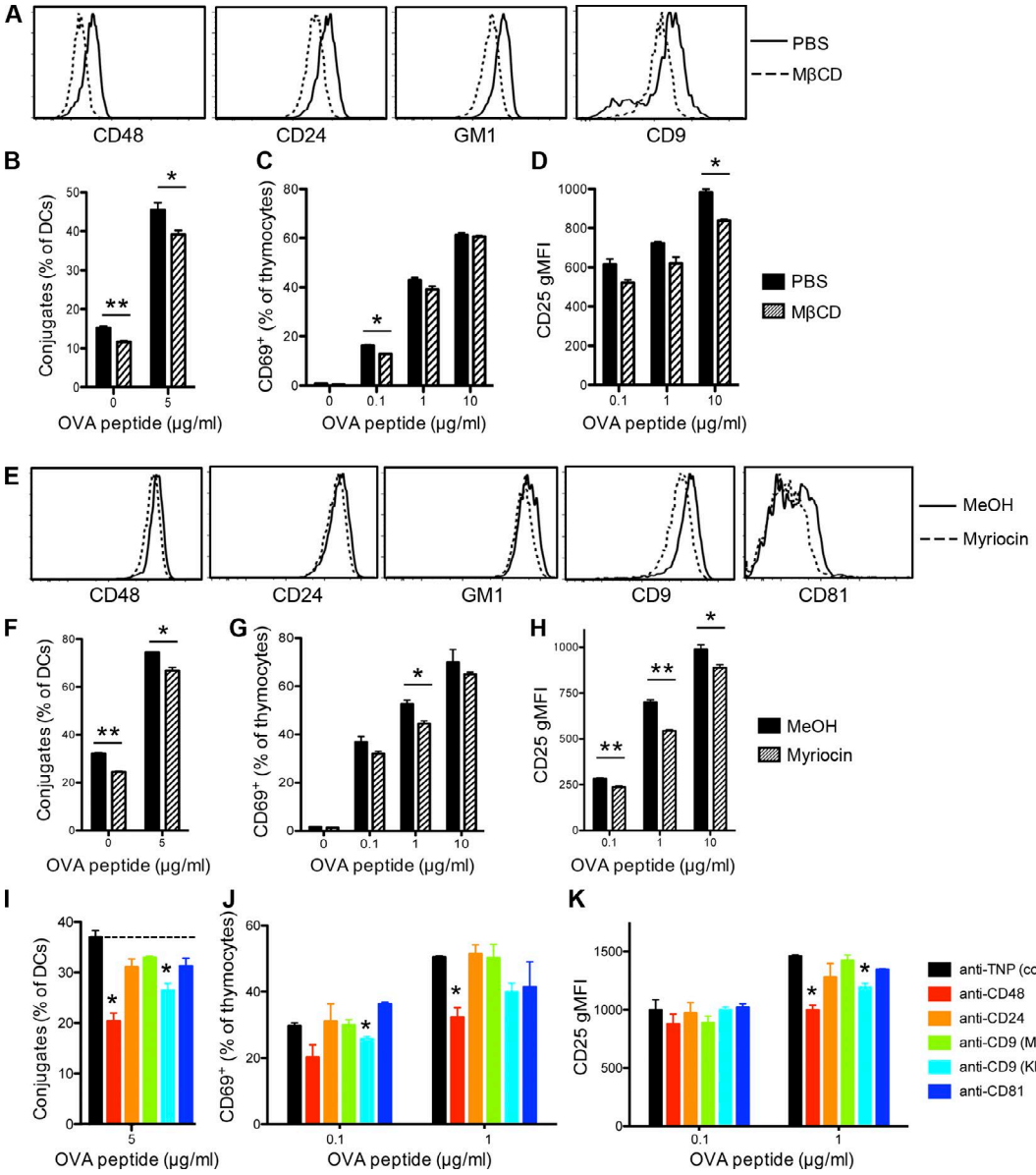

Figure 6. **Lipid raft and tetraspanin web support DC engagement and activation of thymocytes. (A)** BMDCs were treated with PBS or MβCD (4 mM) for 3 h and stained by using monoclonal antibodies raised against indicated molecules except that CTxB was used to detect GM1. **(B–D)** BMDCs pretreated with PBS or MβCD were cultured with $CD4^+CD8^-$ thymocytes isolated from OT-II mice in the presence of increasing concentrations of $OVA_{323-339}$ peptide. The percentage of DCs that formed stable conjugates with thymocytes is shown in B. The percentage of thymocytes that expressed CD69 is shown in C. The level of CD25 expressed in $CD69^+$ thymocytes is shown in D. **(E)** BMDCs were treated with methanol (MeOH) or myriocin (0.5 μg/ml) for 3 d and stained by using monoclonal antibodies raised against indicated molecules except that CTxB was used to detect GM1. **(F–H)** BMDCs treated with MeOH or myriocin were cultured with $CD4^+CD8^-$ thymocytes isolated from OT-II mice in the presence of increasing concentrations of $OVA_{323-339}$ peptide. The percentage of DCs that formed stable conjugates with thymocytes is shown in F. The percentage of thymocytes that expressed CD69 is shown in G. The level of CD25 expressed in $CD69^+$ thymocytes is shown in H. **(I–K)** BMDCs were treated with indicated antibodies for 30 min at 37°C. After washing, the DCs were cultured with $CD4^+CD8^-$ thymocytes isolated from OT-II mice in the presence of increasing concentrations of $OVA_{323-339}$ peptide. The percentage of DCs that formed stable conjugates with thymocytes is shown in I. The percentage of thymocytes that expressed CD69 is shown in J. The level of CD25 expressed in $CD69^+$ thymocytes is shown in K. Statistical analysis was performed in comparison to the cells treated with anti-TNP antibody (control) in I–K. Data represent three to four independent experiments. Error bar represents SEM. *, $P < 0.05$; **, $P < 0.01$.

the ability of MHCII K–deficient DCs to drive Treg cell development. Immature non-Treg $CD4^+$ thymocytes were isolated from $Foxp^{GFP}$OT-II mice, which report Foxp3 by GFP expression. The isolated thymocytes were co-cultured with MHCII K–deficient DCs that had been supplemented with sphingomyelin in the presence of increasing concentrations of ovalbumin peptide. 2 d later, the expression of GFP and CD25 in thymocytes was determined by flow cytometry. We found that the thymocytes cultured with sphingomyelin-treated DCs expressed GFP and CD25, the markers of Treg cells, at a significantly higher frequency than those cultured with vehicle-treated DCs (Fig. 7, E and F). Thus, sphingomyelin supplementation significantly restores the ability of MHCII K–deficient DCs to drive Treg cell development. Collectively, these findings suggest that the alteration of the lipid raft and tetraspanin web was responsible for poor engagement, activation, and Treg cell differentiation

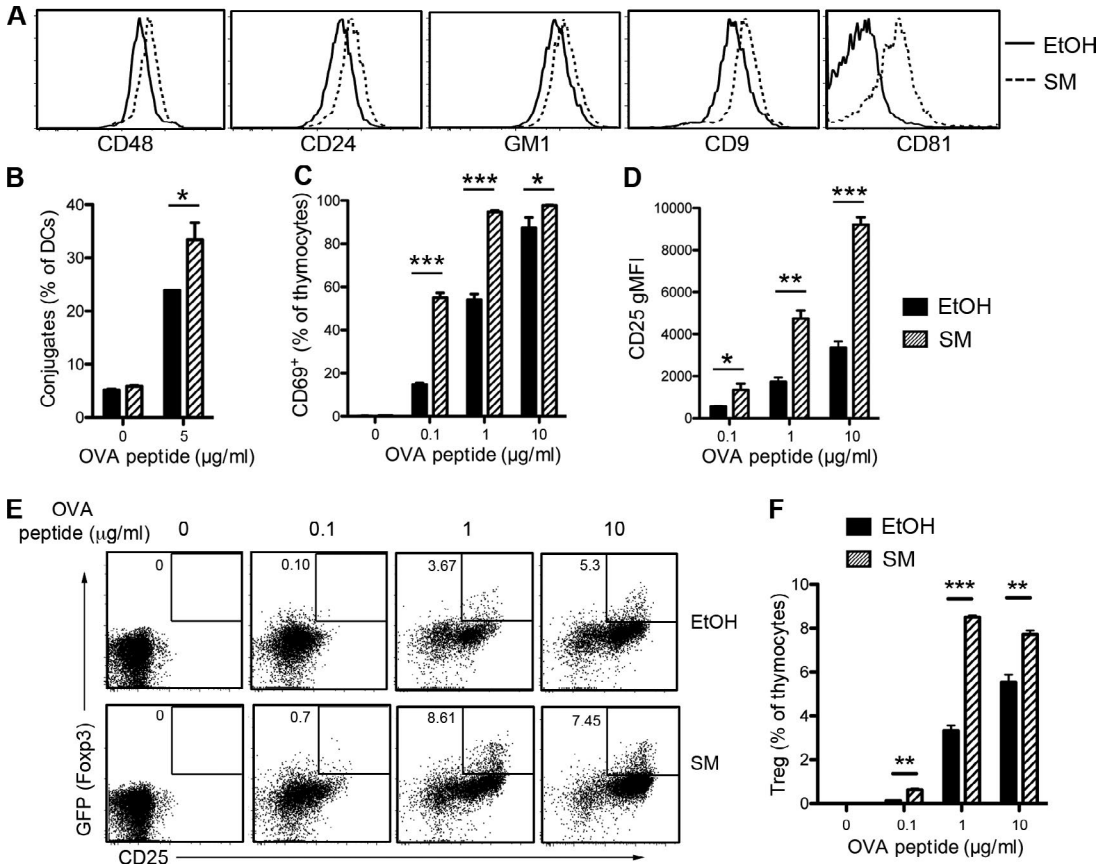

Figure 7. **Sphingomyelin supplementation lessens alteration of the lipid raft and tetraspanin web in MHCII K–deficient DCs and improves the ability of the DCs to engage and activate thymocytes and drive Treg cell differentiation. (A)** BMDCs were derived from MHCII$^{K>R/K>R}$ mice, treated with ethanol (EtOH) or sphingomyelin (SM; 200 μM) for 3 d and stained by using monoclonal antibodies raised against indicated molecules except that CTxB was used to detect GM1. **(B–D)** BMDCs derived from MHCII$^{K>R/K>R}$ mice were treated with EtOH or SM and cultured with CD4$^+$CD8$^-$ thymocytes isolated from OT-II mice in the presence of increasing concentrations of $OVA_{323-339}$ peptide. The percentage of DCs that formed stable conjugates with thymocytes is shown in B. The percentage of thymocytes that expressed CD69 is shown in C. The level of CD25 expressed in CD69$^+$ thymocytes is shown in D. **(E and F)** BMDCs derived from MHCII$^{K>R/K>R}$ mice were treated with EtOH or SM and cultured with GFP$^-$CD4$^+$CD8$^-$ thymocytes isolated from Foxp3^{GFP}OT-II mice in the presence of increasing concentrations of $OVA_{323-339}$ peptide. 2 d later, the expression of GFP and CD25 in the thymocytes was determined by flow cytometry. Representative dot plots are shown in E. The percentage of GFP$^+$CD25$^+$ cells among thymocytes (Treg cells) is shown in F. Data represent two to four independent experiments. Error bars represent SEM. *, P < 0.05; **, P < 0.01; ***, P < 0.005.

of thymocytes by MHCII K–deficient DCs and suggest that sphingolipid may be one of the limiting factors in MHCII K–deficient DCs for maintaining homeostasis of the lipid raft and tetraspanin web against MHCII overcrowding.

The degree of Treg cell deficiency in MARCH1- or MHCII K-deficient mice correlates with the degree of alteration in the lipid raft and tetraspanin web in thymic DCs

The data described so far led to the hypothesis that the failure of MHCII$^{K>R/K>R}$ or MARCH1$^{-/-}$ mice to generate Treg cells to a sufficient number is attributed to the failure of thymic DCs of these mice to maintain homeostasis of the lipid raft and/or tetraspanin web. To test this hypothesis, we first examined thymic DCs derived from WT, MHCII$^{K>R/K>R}$, and MHCII$^{K>R/-}$ for binding by anti-CD48, -CD24, or -CD9 antibodies and CTxB. Similar to what was observed with BMDCs (Fig. 5 A), these antibodies and reagent bound to DCs derived from WT mice the most, and DCs derived from MHCII$^{K>R/K>R}$ mice the least (Fig. 8 A). Then, we compared the ability of these mice to generate antigen-specific Treg cells. The generation of OVA-specific Treg cells was examined in conditions where OVA was expressed in the thymus under the control of a rat insulin promoter (Fig. 8 B) or administered to the circulation (Fig. 8 C; Oh et al., 2013). Although *MHCII*$^{K>R/K>R}$ mice completely failed to generate OVA-specific Treg cells in both conditions, *MHC II*$^{K>R/-}$ mice generated them to an appreciable amount; however, it did not reach the amount generated by WT mice (Fig. 8, B and C). Lastly, we compared the amount of total Treg cells in WT, *MHCII*$^{K>R/K>R}$, and *MHCII*$^{K>R/-}$ mice. Treg cell frequency was reduced by half in *MHCII*$^{K>R/K>R}$ mice compared with WT mice, and it remained similarly low in *MHCII*$^{K>R/-}$ mice (Fig. 8 D).

We performed similar experiments using *MARCH1*$^{-/-}$ and *MARCH1*$^{-/+}$ mice. Thymic DCs of *MARCH1*$^{-/-}$ mice were most poorly bound by anti-CD48, -CD24, or -CD9 antibodies and CTxB, and DCs of MARCH1$^{-/=}$ mice showed markedly improved binding (Fig. 8 E). OVA-specific Treg cells were not generated at all in *MARCH1*$^{-/-}$ mice but were generated in *MARCH1*$^{-/+}$ mice as efficiently as in WT mice both when OVA was expressed in the thymus and when administered to the circulation (Fig. 8, F and G). The total Treg cell amount was also significantly restored in *MARCH1*$^{-/+}$ mice, although it did not reach the level of WT mice (Fig. 8 H). Collectively, Treg development in the thymus decreased in proportion to the degree to

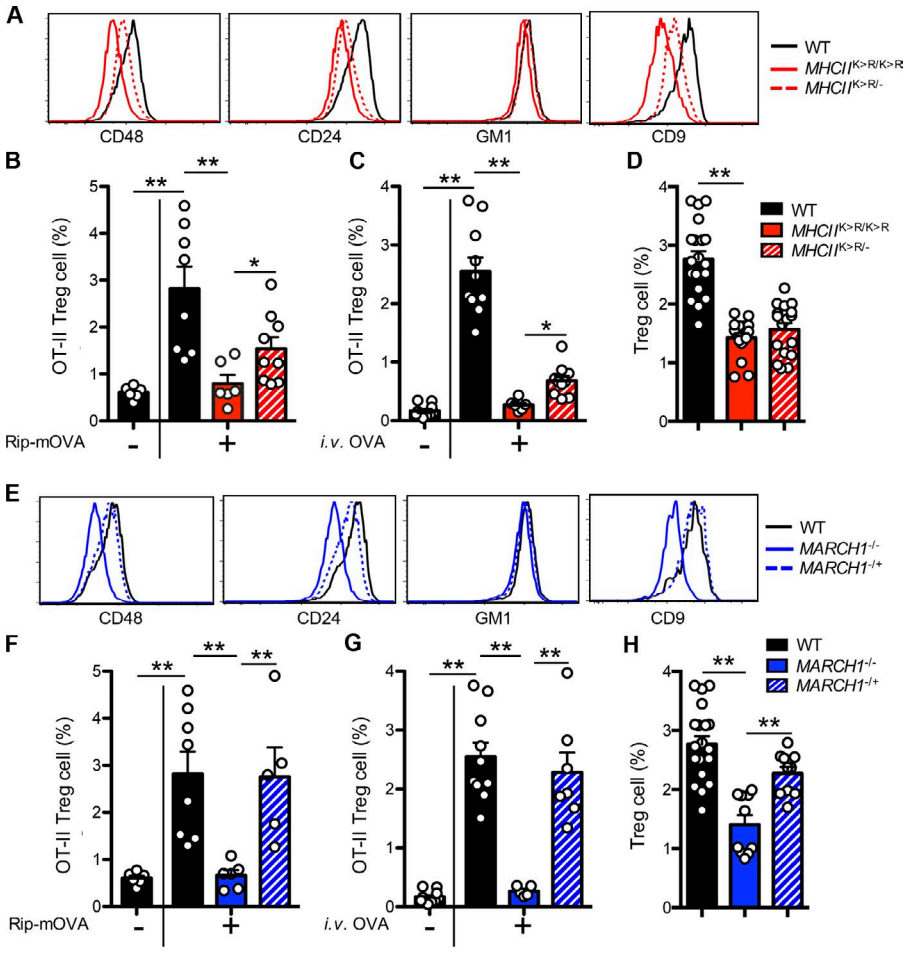

Figure 8. **The degree of Treg cell deficiency in MARCH1 or MHCII K–deficient mice correlates with the degree of alteration in the lipid raft and tetraspanin web in thymic DCs. (A)** DCs were enriched from the thymic digest of WT, MHCII$^{K>R/K>R}$, and MHCII$^{K>R/-}$ mice and stained by using monoclonal antibodies raised against indicated molecules except that CTxB was used to detect GM1. Sirpα$^-$ DCs are shown as the representative. Data represent at least three independent experiments. **(B)** WT (–) and Rip-mOVA (+) transgenic mice were lethally irradiated and transferred with bone marrow isolated from OT-II, MHCII$^{K>R/K>R}$OT-II, or MHC II$^{K>R/-}$OT-II mice. The percentage of OT-II Treg cells among CD4$^+$ thymocytes was determined 6 wk later. **(C)** OT-II, MHCII$^{K>R/K>R}$OT-II, and MHCII$^{K>R/-}$OT-II mice were i.v. injected with PBS (–) or 4 mg ovalbumin (+), and the percentage of OT-II Treg cells among CD4$^+$ thymocytes was determined 3 d later. **(D)** The percentage of Treg cells among CD4$^+$ thymocytes in WT, MHCII$^{K>R/K>R}$, and MHC II$^{K>R/-}$ mice. **(E)** DCs were enriched from the thymic digest of WT, MARCH1$^{-/-}$, and MAR CH1$^{-/+}$ mice and stained by using monoclonal antibodies raised against indicated molecules except that CTxB was used to detect GM1. Sirpα$^-$ DCs are shown as the representative. Data represent at least three independent experiments. **(F)** Mice were treated as described in B, except that bone marrow was isolated from OT-II, MARCH1$^{-/-}$OT-II, and MARCH1$^{-/+}$OT-II mice. **(G)** Mice were treated as described in C, except that OT-II, MARCH1$^{-/-}$OT-II, and MARCH1$^{-/+}$OT-II mice were i.v. injected with PBS (–) or ovalbumin (+). **(H)** The percentage of Treg cells among CD4$^+$ thymocytes in WT, MARCH1$^{-/-}$, and MARCH1$^{-/+}$ mice. Each circle represents an individual mouse. Data were pooled from more than three independent experiments. Error bars represent SEM. *, $P < 0.05$; **, $P < 0.01$.

which the lipid raft and tetraspanin web were altered in thymic DCs. These data suggest the important contribution of the DC lipid raft and tetraspanin web to Treg cell development.

MARCH1 significantly contributes to the diversification of Treg cell repertoire and function

Having found the mechanism by which MARCH1 supports DC selection of Treg cells, we explored the functional significance of this mechanism. Specifically, we determined the contribution that MARCH1 may make to the diversity of Treg cells. MARCH1$^{-/-}$ mice were crossed to transgenic mice with a fixed TCRβ chain (Hsieh et al., 2004). Treg cells were isolated, and the variable TCRα chains were sequenced and analyzed at the individual TCR level (Fig. S5, A and B). We found a substantial loss of Treg cell TCR clones in MARCH1-deficient mice, estimated to comprise ∼33% of the Treg cell TCR clones present in WT mice (Fig. 9, A and B). Remarkably, most of them completely disappeared in MARCH1$^{-/-}$ mice (Fig. 9 A). Some clones were found enriched, although the frequency was as low as 2.3% (Fig. 9, A and B). This finding indicates that MARCH1 plays a significant role in diversifying Treg cell TCR repertoire. We also examined the TCR repertoire of non-Treg CD4$^+$ thymocytes and found that 8.4% of the analyzed TCRs were enriched in MARCH1$^{-/-}$ mice (Figs. S5, C and D). Thus, MARCH1 appears to also play some role in negatively selecting CD4$^+$ thymocytes.

Next, we examined whether the restriction in the repertoire of Treg cells in MARCH1-deficient mice is accompanied by the restriction in their functional capacity. Treg cells isolated from MARCH1-deficient mice suppressed proliferation of CD4$^+$ T cells as effectively as those from WT mice in vitro (Fig. 9 C). To assess Treg cell functionality in physiologically relevant settings, we used two in vivo assays. First, we transferred naive CD4$^+$ T cells to lymphopenic mice (Powrie et al., 1994), which develop wasting disease and inflammatory bowel disease (IBD), which are ameliorated by cotransfer of Treg cells (Mottet et al., 2003). We found that Treg cells derived form MARCH1-deficient mice suppressed both wasting disease and IBD as well as or more effectively than those from WT mice (Fig. 9 D and Fig. S5 E). Second, we used a mouse model of lethal acute graft-versus-host disease (aGVHD) preventable by cotransfer of Treg cells derived from the graft donor (Hoffmann et al., 2002). Transplantation of irradiated BALB/c mice with C57BL/6 mouse bone marrow cells that included CD4$^+$ T cells but not Treg cells resulted in a precipitous death leaving no mice surviving on day 22 after transplantation (Fig. 9 E). However, mice cotransplanted with Treg cells derived from WT C57BL/6 mice were substantially protected from death, resulting in about two thirds of the mice surviving over 36 d after transplantation (Fig. 9 E). In contrast, mice

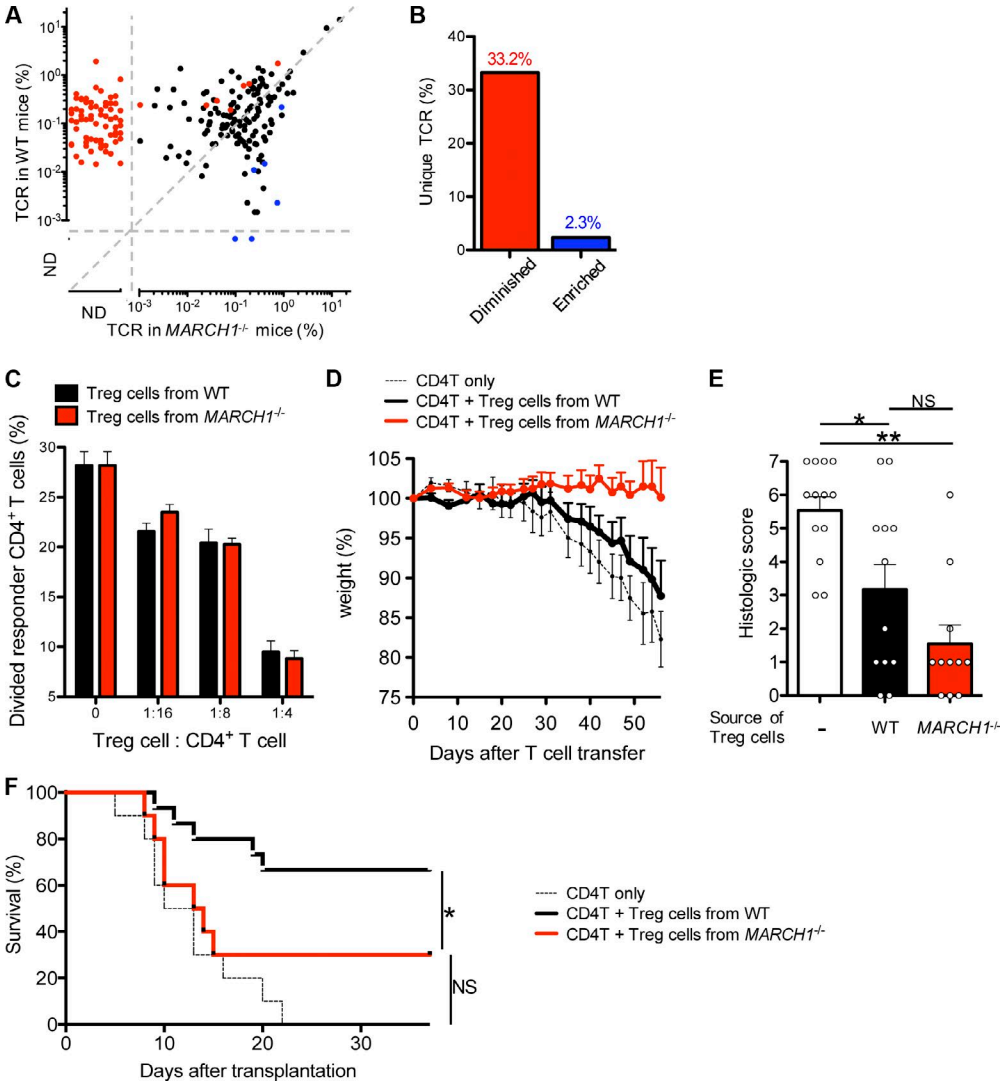

Figure 9. **MARCH1 significantly contributes to the diversification of Treg cell repertoire and function. (A)** Dot plot of unique Treg cell TCR frequencies in MARCH1$^{-/-}$ versus WT mice. Red and blue dots indicate unique TCRs significantly diminished and enriched in MARCH1$^{-/-}$ mice, respectively ($P < 0.075$, Mann-Whitney U test). ND, not detected. **(B)** The percentages of unique Treg cell TCR clones diminished or enriched significantly and more than fivefold in MARCH1$^{-/-}$ mice. **(C)** Treg cells were isolated from thymi of WT or MARCH1$^{-/-}$ mice and mixed with CTV-labeled CD4$^+$ T cells together with anti-CD3 and -CD28 antibody–coated beads. The percentages of CTV-diluted CD4$^+$ T cells were determined. Data represent two independent experiments with triplicates per condition. Error bars represent SEM. **(D and E)** RAG1$^{-/-}$ mice were i.v. injected with naive WT CD4$^+$ T cells alone or together with thymic Treg cells isolated from WT or MARCH1$^{-/-}$ mice. The weight of individual mice was monitored and recorded for 56 d (D). Each curve represents the average weight changes of 12–13 mice per group. Histological scores of distal colons were determined as described in Materials and methods (E). Each circle represents an individual mouse. Data are pooled from three independent experiments. Error bars represent SEM. *, $P < 0.05$; **, $P < 0.01$. **(F)** BALB/c mice were lethally irradiated and i.v. injected with C57BL/6 mouse bone marrow cells depleted of whole T cells and supplemented with C57BL/6 mouse CD4$^+$ T cells alone or together with thymic Treg cells isolated from WT or MARCH1$^{-/-}$ mice. Survival of the mice was monitored for 36 d. Data were pooled from three independent experiments of 10–15 mice per group. Significance was tested by the log-rank test. *, $P < 0.05$.

cotransplanted with Treg cells derived from MARCH1-deficient C57BL/6 mice died as rapidly as those transplanted with CD4$^+$ T cells alone, although some mice managed to live (Fig. 9 E). Thus, Treg cells generated in the absence of MARCH1 are incompetent in suppressing lethal aGVHD. These findings suggest that MAR CH1 contributes to the diversification of the immunosuppressive function of Treg cells as well as TCR repertoire of the cells.

Discussion

The aim of this study was to define the mechanism by which MARCH1-mediated ubiquitination of MHCII supports DC function of selecting natural Treg cells. The presented study indicates that ubiquitin-dependent MHCII turnover is required for DCs to maintain homeostasis of the lipid raft and tetraspanin web in the plasma membrane and that DC ability to engage and activate thymocytes is critically dependent on integrity of these membrane domains. Thus, MARCH1-mediatd MHCII ubiquitination represents a novel quality-control mechanism by which DCs maintain homeostasis of membrane domains that supports Treg cell–selecting function.

Ubiquitination induces endocytosis and lysosomal sorting and degradation of MHCII. Accordingly, when the ubiquitin acceptor lysine of MHCII was mutated in mice, the level of MHC II molecules, including the antigen-loaded MHCII, markedly

increased in DC surface. Yet, the DCs were less efficient at activating antigen-specific thymocytes than WT DCs. By using two independent methods, we showed that this reduced efficiency is attributed not to the absence of ubiquitinated MHCII molecules in the cells but to the presence of too many MHCII molecules. First, we found that the efficiency of MHCII K–deficient DCs at engaging and activating thymocytes was significantly improved when the cells were manipulated to express only one allele of the MHCII. Second, DCs that expressed MHCII via an exogenous promoter that drove MHCII expression much more weakly compared with the endogenous promoter were able to stably engage and strongly activate thymocytes in the absence of the ubiquitin acceptor lysine in MHCII.

We found that MHCII K deficiency resulted in distortion of the lipid raft and tetraspanin web in the plasma membrane of DCs. This distortion was manifested by poor binding of the antibodies or ligands directed to GPI-anchored molecules, GM1, or tetraspanin molecules. This poor binding appears to be largely attributed to conformational changes of the individual molecules driven by MHCII overcrowding in the membrane domains. A recent study has shown that the fraction of GM1 molecules available for CTxB binding changes as the property of GM1-associating membrane changes (Sachl et al., 2015). Another recent study has shown that tetraspanin molecules contain a large intramembrane cavity occupied by cholesterol and that the occupancy of this cavity modulates conformation of tetraspanins (Zimmerman et al., 2016). Possibly, the lipid raft and tetraspanin web in MHCII K–deficient DCs were altered in membrane property by MHCII overcrowding, which resulted in conformational changes in the associated molecules including GM1. Notably, we found that the amount of CD24 present in MHCII K–deficient DCs was slightly lower than that in WT DCs, although the amount of CD24 transcript was identical. We speculate that some of the CD24 molecules in MHCII K–deficient DCs might have been cleaved from the cell surface because phosphatidylinositol-phospholipase C and the angiotensin-converting enzyme, the enzymes capable of cleaving GPI anchor, are activated upon destabilization of the lipid raft (Metz et al., 1994; Sharom and Lehto, 2002; Kondoh et al., 2005). Additional studies using high-resolution microscopy and biophysical experiments would help in understanding the molecular changes occurring in the plasma membrane of MHCII-overcrowded DCs.

The lipid raft and tetraspanin web both promote DC activity of engaging and activating mature $CD4^+$ T cells (Anderson et al., 2000; Kropshofer et al., 2002; Hiltbold et al., 2003). However, the role of these membrane domains in DC activity of engaging, activating, and differentiating $CD4^+$ thymocytes has not been investigated. Cholesterol and sphingolipid both play an important role in maintaining structural integrity of the lipid raft as well as the tetraspanin web (Odintsova et al., 2006). We found that DCs treated with the reagents that reduce cellular levels of cholesterol or sphingolipid were poorly bound by the antibodies or ligand directed to the molecules associated with the lipid raft or tetraspanin web, similarly to what was found in MHCII K–deficient DCs. DCs treated with these reagents also poorly engaged and activated thymocytes compared with untreated DCs. This finding supports that the lipid raft and tetraspanin web were disrupted in MHCII K–deficient DCs and that these membrane domains play an important role in DCs to stably engage and strongly activate thymocytes.

The specific mechanisms by which the lipid raft or tetraspanin web supports DC ability to conjugate and activate thymocytes remain to be further defined. We found that pretreatment with anti-CD48 antibody resulted in a significant reduction in DC ability to engage and activate thymocytes, implicating a role of CD48. CD48 has been shown to bind the adhesion molecule CD2 and facilitate activation of T cells (Kato et al., 1992). A similar mechanism may explain the contribution of CD48 to DC engagement and activation of thymocytes. Pretreatment of DCs with anti-CD9 antibody also resulted in a reduction in DC engagement and activation of thymocytes, although only the KMC8 antibody but not the MZ3 antibody did so. Although the specific epitope recognized by the KMC8 antibody is not known, that epitope may mediate CD9 interaction with some other molecules that promote DC engagement and activation of thymocytes. CD9 and CD81 can interact with multiple integrin molecules in the plasma membrane through their ectodomains (Berditchevski, 2001). CD9 and CD81 are also connected to actin cytoskeleton involving ezrin-radixin-moesin proteins (Sala-Valdés et al., 2006). Thus, these tetraspanin molecules may serve as a linker between adhesion molecules on the surface of DCs and the cytoskeleton in the cortex and promote stable DC interaction with thymocytes. The co-stimulatory molecule CD86 has been shown to be recruited to the lipid raft upon T cell–DC interaction, implicating the role of the lipid raft in T cell stimulatory activity of CD86. Although we did not examine it in this study, MHCII K deficiency may have caused CD86 to poorly associate with the lipid raft in MHCII (K>R) DCs making it unable to provide sufficient co-stimulatory signal to the interacting thymocytes.

We found that MARCH1 deficiency reduced not only the number of Treg cells but also repertoire of the cells. Approximately 33% of Treg TCR clones diminished in MARCH1-deficient mice, and the majority of them were undetectable. We also found some clones of non-Treg $CD4^+$ thymocytes were enriched in MARCH1-deficient mice. However, the frequency of these enriched clones comprised only 8% of total non-Treg $CD4^+$ thymocyte repertoire, implicating a relatively minor role of MARCH1 in negative selection over Treg cell development. Both negative selection and Treg cell development are promoted by high-affinity interaction between DCs and thymocytes. However, a recent study has revealed that the TCR affinity threshold to elicit negative selection is ∼100-fold higher than that of Treg cell development. This study also showed that Treg cells can develop in a broad ∼1,000-fold range of TCR affinity. This extremely broad range of Treg cell affinity may be attributed to the role of the lipid raft and tetraspanin web in promoting DC engagement and activation of thymocytes. We found that the Treg cells generated in the absence of MARCH1 sufficiently suppressed wasting disease and IBD but not aGVHD. Previous studies have shown that the alloantigen-specific Treg cells suppressed alloreactive effector T cells more effectively than polyclonal Treg cells in vitro (Chen et al., 2009; Veerapathran et al., 2013). Alloantigen-specific Treg cells also suppressed aGVHD more effectively than polyclonal Treg cells when transferred to mice that received allotransplantation (Yamazaki et al., 2006; Golshayan et al., 2007). Thus, MARCH1 may play a particularly important role in the development of Treg cells reactive to alloantigens.

In conclusion, this study reveals an unexpected role of MARCH1 and MHCII ubiquitination in DC membrane homeostasis and Treg cell–selecting function. The dependency of MARCH1 and MHCII ubiquitination in other DC functions, such as development of effector T cells, would be an important remaining topic to be studied.

Materials and methods

Mice

C57BL/6, BALB/c, B6.PL-Thy1^{a}/CyJ (Thy1.1), B6.129S2-H2$^{dlAb1\text{-}Ea}$/J (MHCII$^{-/-}$), B6.129S2-Tcra^{tm1Mom}/J (TCRα$^{-/-}$), B6.129S7-Rag1$^{tm/1Mom}$/J (Rag1$^{-/-}$), B6.Cg-Tg(Itgax-cre)1-1Reiz/J (CD11c-CRE), B6.Cg-Tg(UBC-cre/ERT2)1Ejb (ERT-CRE), B6;SJL-Tg(ACTFLPe)9205-Dym/J (ACT-FLP), B6.Cg-Tg(TcraTcrb)425Cbn/J (OT-II), and B6.SJL-Ptprc^{a} Pepc^{b}/BoyJ (BoyJ) mice were purchased from the Jackson Laboratory. B6.129-H20Ab1tm1GruN12 (MHCIIβ$^{-/-}$) mice were purchased from Taconic. MHCII$^{K>R/K>R}$ (Oh et al., 2013), MARCH1$^{-/-}$ (Matsuki et al., 2007), Rip-mOVA (Kurts et al., 1996), foxp3^{GFP} (Haribhai et al., 2007), and TCli β transgenic (Hsieh et al., 2004) mice were described previously. All mice were maintained in the University of California, San Francisco (UCSF), mouse facility, and all animal studies were performed according to protocols approved by the UCSF Institutional Animal Ethics Committee.

Antibodies and reagents

The following antibodies were purchased from BioLegend, eBioscience, or BD Biosciences and used for flow cytometry or enrichment: FITC-Sirpα, PE/Cy7-Sirpα, PerCP/Cy5.5-B220, APC-EpCAM, PE-CD11c, PE/Cy7-CD11c, Brilliant Violet 605-CD11c, Pacific Blue-IA/IE, FITC-CD8α, Alexa700-CD8α, PE-V$_{\alpha}$2, APC-V$_{\alpha}$2, APC-V$_{\beta}$5, PE-V$_{\beta}$6, PE-Foxp3, Pacific Blue-Foxp3, PerCP/Cy5.5-Thy1.1, APC-TCRβ, PE-CD69, PE/Cy7-CD69, Brilliant Violet 605-CD4, APC-CD25, Brilliant Violet 605-CD25, Brilliant Violet 785-CD25, FITC-CD45RB, APC-ICAM1, PR-CD9, PE-CD81, APC-CD48, PE/Cy7-CD24, APC-CD24, PE-CD71, PE/Cy7-CD45, APC-streptavidin, Biotin-Thy1.2, Biotin-CD8β, Biotin-CD25, and Biotin-B220. Alexa647-CTxB subunit was purchased from Molecular Probes. For Western blotting, the following clones were used: MHCII β chain (Bett; homemade), CD48 (OX-78; Serotec), CD24 (M1/69; BioLegend), actin (A2066; Sigma), CD9 (LMC8; eBioscience), and CD81 (Eat2; BioLegend), and HRP-conjugated secondary antibodies (anti-rat, anti-rabbit, and anti-hamster) were purchased from Jackson ImmunoResearch or BIOSOURCE. Myriocin, MβCD, cholesterol, sphingomyelin, and 4-hydroxy-tamoxifen were purchased from Sigma.

Generation of MARCH1$^{fl/fl}$CD11c-CRE mice

Embryonic stem cells containing targeted conditional alleles of MARCH1 were purchased from EUCOMM and transplanted to C57BL/6 mice in the UC Davis Mouse Biology Program. Two chimeric mice were generated, and both mice successfully provided germ-line transmission. One of them was crossed with Act-FLP transgenic mice to remove the FRT flanking region and subsequently with CD11c-CRE or ERT-Cre transgenic mice to remove the loxP-flanking region. See Fig. S1.

Isolation of thymic DCs

Thymi were isolated and digested with 125 mg/ml collagenase D and 62.5 µg/ml DNaseI for 20 min with gentle rocking at 37°C. Digests were filtered through a 70-µm filter cap strainer (BD Falcon), resuspended in 1 ml high-density (1.115 g/ml) Percoll solution (GE healthcare), and layered with 1 ml low-density (1.065 g/ml) Percoll solution followed by 1 ml PBS. This Percoll gradient was centrifuged at 2,700 rpm for 30 min at 4°C to enrich antigen-presenting cells. Cells between the PBS and low-density Percoll layer were isolated and used for flow cytometric analysis as described in our previous study (Oh et al., 2013) or enriched further by using magnetic beads conjugated with anti-CD11c antibody (Miltenyi Biotec).

Culture of BMDCs and isolation of conventional DCs (cDCs)

Bone marrow cells were cultured with RPMI media supplemented with 10% FBS and 100 ng/ml Flt3-ligand (Peprotech) for 12 d. For isolation of cDCs, cells were harvested and preincubated with Fc block for 10 min on ice in MACS buffer (PBS with 1% BSA and 2 mM EDTA) and then with biotin-B220 antibody and streptavidin–magnetic bead to remove plasmacytoid DCs. These cDCs were further purified by cell sorting before RNA isolation, Western blotting, and sucrose gradient fractionation.

Retroviral transduction of BMDCs

The retrovirus encoding MHCII WT, MHCII (K>R) mutant, or CD86 (K>R) mutant was generated as previously described (Shin et al., 2006; Baravalle et al., 2011). The generated virus was mixed with polybrene (10 µg/ml) and added to BMDCs on the second day of culture. The BMDCs were spun at 2,500 rpm for 2 h at RT, and the supernatant was replaced with the Flt3-ligand-containing media. Cells were cultured for an additional 10 to 12 d.

Quantitative PCR

Genomic DNA was purified using the PureLink genomic DNA Mini kit (Invitrogen) from Sirpα^{-} DCs (CD11c^{+}MHCII^{+}B220^{-} autofluorescence^{-}Sirpα^{-}), Sirpα^{+} DCs (CD11c^{+}MHCII^{+}B220^{-} autofluorescence^{-}Sirpα^{+}), B cells (B220^{+}MHCII^{+}CD11c^{-}), and thymic epithelial cells (EpCAM^{+}MHCII^{+}CD11c^{-}B220^{-}) isolated from the thymi of MARCH1$^{fl/fl}$ and MARCH1$^{fl/fl}$ CD11c-CRE mice. Quantitate PCR was performed on an Eppendorf realplex system by using SYBR Green reagents and the primer pair spanning 3′ LoxP site (5′ primer, AGCTGTAAGAACTGACCTCAA; 3′ primer, GGAGGA TGCTTGTCCTGTAAA). See also Fig. S1. Total RNAs were isolated from sorted cDCs by TRIzol (Invitrogen). The first-strand cDNA was generated by using SuperScript III system (Invitrogen) with the use of oligo dT as primer. Quantitative PCR was performed by using primers specific for CD48, CD24, Sptlc2, CD9, and HPRT (https://pga.mgh.harvard.edu/primerbank/).

Flow cytometry and cell sorting

Cells were incubated with fluorophore-conjugated antibodies in FACS buffer (1% BSA in PBS) containing propidium iodide solution (BioLegend) for 30 min on ice. When staining DCs, cells were preincubated with CD16/32 Fc block antibody (UCSF Cell Culture Facility). Foxp3 was stained by using Foxp3/Transcription Factor Staining Buffer Set as instructed (eBioscience). Samples were analyzed and sorted by the FACS LSRII system (BD Biosciences) and BD FACS Aria3 Cell Sorter (BD Biosciences), respectively.

Thymocyte conjugation and activation assay

CD4^{+} thymocytes were isolated through negative selection by using biotin-CD8β and biotin-CD25 antibodies and streptavidin-conjugated magnetic beads (Stemcell Technologies) from Thy1.1 OT-II mice. Isolated cells (1×10^{5}) were co-cultured with thymic DCs (2×10^{4}) or BMDCs (2×10^{4}) in the presence of increasing amounts of OVA protein or OVA$_{323\text{-}339}$ peptide. Thymocyte conjugation was assayed after 3 h by centrifuging cell mixtures and vortexing pellets for 5 s at the highest speed before fixation and antibody staining. The percentage of Thy1.1^{+}V$_{\beta}$5^{+} cells among CD11c^{+}MHCII^{+} population was determined by flow cytometry. Thymocyte activation was assayed after 24 h by determining the percentages of CD69^{+} and the geometric mean fluorescence intensity of CD25 of CD69^{+} among Thy1.1^{+}V$_{\beta}$5^{+} population by flow cytometry.

Western blotting

cDCs isolated from WT and MHCII$^{K>R/K>R}$ BMDCs were boiled in Laemmli buffer for 5 min and run on SDS-PAGE. Gels were transferred to polyvinylidene difluoride membrane, and the membranes were preincubated with blocking solution (5% nonfat milk in PBST [PBS with 0.1% Tween-20]) with gentle agitation for at least 30 min, which was followed by primary antibody incubation for overnight at 4°C and secondary antibody incubation for 1 h at RT. ECL reaction was performed, and the membrane was imaged by using ChemiDoc XRS+ (Bio-Rad).

Sucrose gradient fractionation

BMDCs were lysed with MES-buffered saline (150 mM NaCl and 25 mM Mes, pH 6.2) containing 1% Brij-58 (Surfact-Amps 58; Thermo Scientific) in the presence of Halt protease inhibitor Cocktail (Thermo Scientific). The lysates were adjusted to 40% sucrose and overlaid over a 35–5% sucrose gradient and centrifuged at 45,000 rpm for 18 h. 10 equal fractions were collected from the top of the gradient and used for Western blot analyses.

Bone marrow transplantation

Bone marrow cells were isolated from femurs and/or tibiae of the donor mice. Recipient mice were lethally irradiated (1,200 rad) and intravenously injected with 3–5 × 10^6 bone marrow cells. Mice were examined 6 wk later.

Treg cell TCR repertoire sequencing

Treg cell and non-Treg CD4$^+$ thymocyte TCR repertoire sequencing was performed as previously described (Perry et al., 2014). In brief, CD4$^+$CD8$^-$GFP$^+$CD25$^+$CD24$^-$V$_\beta$6$^+$V$_\alpha$2$^+$ Treg cells and CD4$^+$CD8$^-$GFP$^-$CD25$^-$CD24$^-$V$_\beta$6$^+$V$_\alpha$2$^+$ non-Treg CD4$^+$ thymocytes were isolated from thymi of 5- to 6-wk-old TCliβ;foxp3-EGFP;TCRα$^{-/+}$ mice and MARCH1$^{-/-}$;TCliβ;foxp3-EGFP;TCRα$^{-/+}$ mice. cDNA was synthesized by using a TCRα specific primer (Perry et al., 2014) and used for amplification of the TRAV14 gene segment. The TRAV14 PCR proceeded in two steps; the first involved the TRAV14-specific primer (5′-GCAGCAGGTGAGACAAAG-3′) and an extension sequence (5′-ACACGACGCTCTTCCGATCT-3′) with a Cα-specific reverse primer (5′-TCAGCAGGAGGATTCGGAGTCCCA-3′). The second step used a nested PCR with a forward primer containing the MiSeq Universal Adapter sequence and a sequence complementary to the common extension sequence from PCR 1 with a reverse primer containing the Miseq Universal Adapter, an 8-bp hamming code, and a sequence complementary to a portion of the Cα-specific reverse primer. Resulting amplicons were sequenced via 250-bp paired-end reads by using a MiSeq sequencer (Illumina). Sequences were demultiplexed and analyzed using blastn to identify the TRAV and TRAJ gene segments by using the IMGT database (Giudicelli et al., 2006). Downstream analysis was performed as reported previously (Perry et al., 2014). See also Fig. S5 (A and B).

In vitro Treg cell suppression assay

CD25$^-$CD4$^+$CD8$^-$ conventional CD4$^+$ T cells (2.5 × 10^4 cells) sorted from BoyJ (CD45.1$^+$) mice spleens were labeled with Celltrace Violet (CTV; Invitrogen) and mixed with Treg cells (CD25$^+$CD4$^+$CD8$^-$) sorted from thymi of WT or MARCH1$^{-/-}$ mice to various ratios. The cell mixtures were added with 10^4 beads conjugated with anti-CD3 and anti-CD28 antibodies and cultured in 37°C for 3 d. The percentages of CD45.1$^+$ conventional CD4$^+$ T cells with their CTV diluted were determined by flow cytometry.

Treg cell–dependent suppression of wasting disease and IBD

Naive CD4$^+$ T cells (CD45RB^{hi}CD25$^-$CD4$^+$CD8$^-$) were isolated from WT mouse spleens and lymph nodes and injected into 9- to 12-wk-old Rag1$^{-/-}$ mice (4–5 × 10^5 cells per mouse). Some mice were also injected with Treg cells isolated from WT or MARCH1$^{-/-}$ mice thymi (2–2.5 × 10^5 cells per mouse). Mice were weighed every 2–3 d. Mice were euthanized on day 56, and distal colons were stained by using hematoxylin and eosin. The pathology was scored as follows: mucosal damage (0, none; 1, discrete lymphoepithelial lesions; 2, diffuse crypt elongation; or 3, extensive crypt elongation or mucosal ulceration), immune cell infiltration (0, none; 1, widely scattered leukocytes or focal aggregates; 2, confluent leukocytes extending into submucosa with focal effacement of the mucosa; or 3, leukocyte infiltration with transmural extension), and crypt abscess (0, absent; or 1, present; Yamaji et al., 2012). Values for each slide were summed for a total score of 0–7.

Treg cell–dependent suppression of lethal acute GVHD.

T cell–depleted C57BL/6 mouse bone marrow cells were mixed with conventional CD4$^+$ T cells (CD25$^-$CD4$^+$CD8$^-$) isolated from C57BL/6 mouse spleens and lymph nodes. The cell mixtures were injected into lethally irradiated (850 rad) 8- to 10-wk-old BALB/c mice (2–3 × 10^6 T cell–depleted bone marrow cells and 4–5 × 10^5 conventional CD4$^+$ T cells per mouse). Some mice were also injected with Treg cells isolated from WT and MARCH1$^{-/-}$ mice thymi (2–2.5 × 10^5 cells per mouse). Viability of mice was monitored every day for record.

Software and statistical analyses

Flow cytometry data were analyzed by FlowJo. Graphs were drawn by PRISM (GraphPad). Unpaired two-tailed Student's *t* test was performed to assess the significance unless stated otherwise. R v3.2.3 was used for graphical and statistical analysis of TCR repertoire data. The R package DESeq2 (v1.10.3) was used for differential TCR expression analysis, and vegan (v2.3-5) for dimensional analysis, rarefaction, and visualization.

Online supplemental material

Fig. S1 shows the map of the MARCH1 exon6-targeting construct used to generate MARCH1$^{fl/fl}$ mice. Fig. S2 shows the surface expression of MHCII, CD86, CD80, and ICAM1 in thymic DCs of WT, MARCH1$^{-/-}$, or MHCII$^{K>R/K>R}$ mice. Fig. S3 shows the association of MHCII with the lipid raft in WT and MHCII$^{K>R/K>R}$ DCs. Fig. S4 shows that the excessive accumulation of CD86 in DCs does not alter the lipid raft or tetraspanin web. Fig. S5 provides additional details related to the TCR repertoire analysis and representative images of colonic inflammation of the IBD mouse model.

Acknowledgments

We thank M. Onizawa and A. Ma for advise on the IBD mouse model, C. Castellanos for critically reading the manuscript, and I. Mellman for providing the MHCII$^{K>R/K>R}$ mice.

This work was supported by National Institutes of Health (GM105800 to J.-S. Shin) and University of California, San Francisco, Sandler Asthma Basic Research Center (J.-S. Shin).

The authors declare no competing financial interests.

Author contributions: J. Oh and J.-S. Shin designed experiments and wrote the manuscript. J. Oh, J.S.A. Perry, H. Pua, N. Irgens-Möller, and J.-S. Shin performed experiments. J. Oh, J.-S. Shin, J.S.A. Perry, and C.-S. Hsieh analyzed the data. S. Ishido provided MARCH1$^{-/-}$ mice.

Submitted: 22 November 2016
Revised: 25 October 2017
Accepted: 8 January 2018

References

Anderson, H.A., and P.A. Roche. 2015. MHC class II association with lipid rafts on the antigen presenting cell surface. *Biochim. Biophys. Acta.* 1853:775–780. https://doi.org/10.1016/j.bbamcr.2014.09.019

Anderson, H.A., E.M. Hiltbold, and P.A. Roche. 2000. Concentration of MHC class II molecules in lipid rafts facilitates antigen presentation. *Nat. Immunol.* 1:156–162. https://doi.org/10.1038/77842

Baravalle, G., H. Park, M. McSweeney, M. Ohmura-Hoshino, Y. Matsuki, S. Ishido, and J.S. Shin. 2011. Ubiquitination of CD86 is a key mechanism in regulating antigen presentation by dendritic cells. *J. Immunol.* 187:2966–2973. https://doi.org/10.4049/jimmunol.1101643

Bartee, E., M. Mansouri, B.T. Hovey Nerenberg, K. Gouveia, and K. Früh. 2004. Downregulation of major histocompatibility complex class I by human ubiquitin ligases related to viral immune evasion proteins. *J. Virol.* 78:1109–1120. https://doi.org/10.1128/JVI.78.3.1109-1120.2004

Berditchevski, F. 2001. Complexes of tetraspanins with integrins: more than meets the eye. *J. Cell Sci.* 114:4143–4151.

Björkholm, P., A.M. Ernst, M. Hacke, F. Wieland, B. Brügger, and G. von Heijne. 2014. Identification of novel sphingolipid-binding motifs in mammalian membrane proteins. *Biochim. Biophys. Acta.* 1838:2066–2070. https://doi.org/10.1016/j.bbamem.2014.04.026

Charrin, S., S. Manié, C. Thiele, M. Billard, D. Gerlier, C. Boucheix, and E. Rubinstein. 2003. A physical and functional link between cholesterol and tetraspanins. *Eur. J. Immunol.* 33:2479–2489. https://doi.org/10.1002/eji.200323884

Charrin, S., S. Jouannet, C. Boucheix, and E. Rubinstein. 2014. Tetraspanins at a glance. *J. Cell Sci.* 127:3641–3648. https://doi.org/10.1242/jcs.154906

Chen, L.C., J.C. Delgado, P.E. Jensen, and X. Chen. 2009. Direct expansion of human allospecific FoxP3+CD4+ regulatory T cells with allogeneic B cells for therapeutic application. *J. Immunol.* 183:4094–4102. https://doi.org/10.4049/jimmunol.0901081

Corcoran, K., M. Jabbour, C. Bhagwandin, M.J. Deymier, D.L. Theisen, and L. Lybarger. 2011. Ubiquitin-mediated regulation of CD86 protein expression by the ubiquitin ligase membrane-associated RING-CH-1 (MARCH1). *J. Biol. Chem.* 286:37168–37180. https://doi.org/10.1074/jbc.M110.204040

De Gassart, A., V. Camosseto, J. Thibodeau, M. Ceppi, N. Catalan, P. Pierre, and E. Gatti. 2008. MHC class II stabilization at the surface of human dendritic cells is the result of maturation-dependent MARCH I down-regulation. *Proc. Natl. Acad. Sci. USA.* 105:3491–3496. https://doi.org/10.1073/pnas.0708874105

Giudicelli, V., P. Duroux, C. Ginestoux, G. Folch, J. Jabado-Michaloud, D. Chaume, and M.P. Lefranc. 2006. IMGT/LIGM-DB, the IMGT comprehensive database of immunoglobulin and T cell receptor nucleotide sequences. *Nucleic Acids Res.* 34:D781–D784. https://doi.org/10.1093/nar/gkj088

Golshayan, D., S. Jiang, J. Tsang, M.I. Garin, C. Mottet, and R.I. Lechler. 2007. In vitro-expanded donor alloantigen-specific CD4+CD25+ regulatory T cells promote experimental transplantation tolerance. *Blood.* 109:827–835. https://doi.org/10.1182/blood-2006-05-025460

Hanada, K. 2003. Serine palmitoyltransferase, a key enzyme of sphingolipid metabolism. *Biochim. Biophys. Acta.* 1632:16–30. https://doi.org/10.1016/S1388-1981(03)00059-3

Haribhai, D., W. Lin, L.M. Relland, N. Truong, C.B. Williams, and T.A. Chatila. 2007. Regulatory T cells dynamically control the primary immune response to foreign antigen. *J. Immunol.* 178:2961–2972. https://doi.org/10.4049/jimmunol.178.5.2961

Hiltbold, E.M., N.J. Poloso, and P.A. Roche. 2003. MHC class II-peptide complexes and APC lipid rafts accumulate at the immunological synapse. *J. Immunol.* 170:1329–1338. https://doi.org/10.4049/jimmunol.170.3.1329

Hoffmann, P., J. Ermann, M. Edinger, C.G. Fathman, and S. Strober. 2002. Donor-type CD4(+)CD25(+) regulatory T cells suppress lethal acute graft-versus-host disease after allogeneic bone marrow transplantation. *J. Exp. Med.* 196:389–399. https://doi.org/10.1084/jem.20020399

Hsieh, C.S., Y. Liang, A.J. Tyznik, S.G. Self, D. Liggitt, and A.Y. Rudensky. 2004. Recognition of the peripheral self by naturally arising CD25+ CD4+ T cell receptors. *Immunity.* 21:267–277. https://doi.org/10.1016/j.immuni.2004.07.009

Hsieh, C.S., H.M. Lee, and C.W. Lio. 2012. Selection of regulatory T cells in the thymus. *Nat. Rev. Immunol.* 12:157–167.

Kato, K., M. Koyanagi, H. Okada, T. Takanashi, Y.W. Wong, A.F. Williams, K. Okumura, and H. Yagita. 1992. CD48 is a counter-receptor for mouse CD2 and is involved in T cell activation. *J. Exp. Med.* 176:1241–1249. https://doi.org/10.1084/jem.176.5.1241

Klein, L., B. Kyewski, P.M. Allen, and K.A. Hogquist. 2014. Positive and negative selection of the T cell repertoire: what thymocytes see (and don't see). *Nat. Rev. Immunol.* 14:377–391. https://doi.org/10.1038/nri3667

Kondoh, G., H. Tojo, Y. Nakatani, N. Komazawa, C. Murata, K. Yamagata, Y. Maeda, T. Kinoshita, M. Okabe, R. Taguchi, and J. Takeda. 2005. Angiotensin-converting enzyme is a GPI-anchored protein releasing factor crucial for fertilization. *Nat. Med.* 11:160–166. https://doi.org/10.1038/nm1179

Kropshofer, H., S. Spindeldreher, T.A. Röhn, N. Platania, C. Grygar, N. Daniel, A. Wölpl, H. Langen, V. Horejsi, and A.B. Vogt. 2002. Tetraspan microdomains distinct from lipid rafts enrich select peptide-MHC class II complexes. *Nat. Immunol.* 3:61–68. https://doi.org/10.1038/ni750

Kurts, C., W.R. Heath, F.R. Carbone, J. Allison, J.F. Miller, and H. Kosaka. 1996. Constitutive class I-restricted exogenous presentation of self antigens in vivo. *J. Exp. Med.* 184:923–930. https://doi.org/10.1084/jem.184.3.923

Lehner, P.J., S. Hoer, R. Dodd, and L.M. Duncan. 2005. Downregulation of cell surface receptors by the K3 family of viral and cellular ubiquitin E3 ligases. *Immunol. Rev.* 207:112–125. https://doi.org/10.1111/j.0105-2896.2005.00314.x

Matsuki, Y., M. Ohmura-Hoshino, E. Goto, M. Aoki, M. Mito-Yoshida, M. Uematsu, T. Hasegawa, H. Koseki, O. Ohara, M. Nakayama, et al. 2007. Novel regulation of MHC class II function in B cells. *EMBO J.* 26:846–854. https://doi.org/10.1038/sj.emboj.7601556

Metz, C.N., G. Brunner, N.H. Choi-Muira, H. Nguyen, J. Gabrilove, I.W. Caras, N. Altszuler, D.B. Rifkin, E.L. Wilson, and M.A. Davitz. 1994. Release of GPI-anchored membrane proteins by a cell-associated GPI-specific phospholipase D. *EMBO J.* 13:1741–1751.

Mottet, C., H.H. Uhlig, and F. Powrie. 2003. Cutting edge: Cure of colitis by CD4+CD25+ regulatory T cells. *J. Immunol.* 170:3939–3943. https://doi.org/10.4049/jimmunol.170.8.3939

Odintsova, E., T.D. Butters, E. Monti, H. Sprong, G. van Meer, and F. Berditchevski. 2006. Gangliosides play an important role in the organization of CD82-enriched microdomains. *Biochem. J.* 400:315–325. https://doi.org/10.1042/BJ20060259

Oh, J., and J.S. Shin. 2015. Molecular mechanism and cellular function of MHC II ubiquitination. *Immunol. Rev.* 266:134–144. https://doi.org/10.1111/imr.12303

Oh, J., N. Wu, G. Baravalle, B. Cohn, J. Ma, B. Lo, I. Mellman, S. Ishido, M. Anderson, and J.S. Shin. 2013. MARCH1-mediated MHCII ubiquitination promotes dendritic cell selection of natural regulatory T cells. *J. Exp. Med.* 210:1069–1077. https://doi.org/10.1084/jem.20122695

Ohmura-Hoshino, M., E. Goto, Y. Matsuki, M. Aoki, M. Mito, M. Uematsu, H. Hotta, and S. Ishido. 2006. A novel family of membrane-bound E3 ubiquitin ligases. *J. Biochem.* 140:147–154. https://doi.org/10.1093/jb/mvj160

Perry, J.S.A., C.J. Lio, A.L. Kau, K. Nutsch, Z. Yang, J.I. Gordon, K.M. Murphy, and C.S. Hsieh. 2014. Distinct contributions of Aire and antigen-presenting-cell subsets to the generation of self-tolerance in the thymus. *Immunity.* 41:414–426. https://doi.org/10.1016/j.immuni.2014.08.007

Powrie, F., M.W. Leach, S. Mauze, S. Menon, L.B. Caddle, and R.L. Coffman. 1994. Inhibition of Th1 responses prevents inflammatory bowel disease in scid mice reconstituted with CD45RBhi CD4+ T cells. *Immunity.* 1:553–562. https://doi.org/10.1016/1074-7613(94)90045-0

Roy, K., M. Ghosh, T.K. Pal, S. Chakrabarti, and S. Roy. 2013. Cholesterol lowering drug may influence cellular immune response by altering MHC II function. *J. Lipid Res.* 54:3106–3115. https://doi.org/10.1194/jlr.M041954

Sachl, R., M. Amaro, G. Aydogan, A. Koukalova, and I.I. Mikhalyov, I.A. Boldyrev, J. Humpoličkova, and M. Hof. 2015. On multivalent receptor activity of GM1 in cholesterol containing membranes. *Biochim. Biophys. Acta.* 1853:850–857.

Sala-Valdés, M., A. Ursa, S. Charrin, E. Rubinstein, M.E. Hemler, F. Sánchez-Madrid, and M. Yáñez-Mó. 2006. EWI-2 and EWI-F link the tetraspanin web to the actin cytoskeleton through their direct association with ezrin-radixin-moesin proteins. *J. Biol. Chem.* 281:19665–19675. https://doi.org/10.1074/jbc.M602116200

Sharom, F.J., and M.T. Lehto. 2002. Glycosylphosphatidylinositol-anchored proteins: structure, function, and cleavage by phosphatidylinositol-specific phospholipase C. *Biochem. Cell Biol.* 80:535–549. https://doi.org/10.1139/o02-146

Shin, J.S., M. Ebersold, M. Pypaert, L. Delamarre, A. Hartley, and I. Mellman. 2006. Surface expression of MHC class II in dendritic cells is controlled by regulated ubiquitination. *Nature.* 444:115–118. https://doi.org/10.1038/nature05261

Simons, K., and J.L. Sampaio. 2011. Membrane organization and lipid rafts. *Cold Spring Harb. Perspect. Biol.* 3:a004697. https://doi.org/10.1101/cshperspect.a004697

Stritesky, G.L., S.C. Jameson, and K.A. Hogquist. 2012. Selection of self-reactive T cells in the thymus. *Annu. Rev. Immunol.* 30:95–114. https://doi.org/10.1146/annurev-immunol-020711-075035

Unternaehrer, J.J., A. Chow, M. Pypaert, K. Inaba, and I. Mellman. 2007. The tetraspanin CD9 mediates lateral association of MHC class II molecules on the dendritic cell surface. *Proc. Natl. Acad. Sci. USA.* 104:234–239. https://doi.org/10.1073/pnas.0609665104

van Niel, G., R. Wubbolts, T. Ten Broeke, S.I. Buschow, F.A. Ossendorp, C.J. Melief, G. Raposo, B.W. van Balkom, and W. Stoorvogel. 2006. Dendritic cells regulate exposure of MHC class II at their plasma membrane by oligoubiquitination. *Immunity.* 25:885–894. https://doi.org/10.1016/j.immuni.2006.11.001

Veerapathran, A., J. Pidala, F. Beato, B. Betts, J. Kim, J.G. Turner, M.K. Hellerstein, X.Z. Yu, W. Janssen, and C. Anasetti. 2013. Human regulatory T cells against minor histocompatibility antigens: ex vivo expansion for prevention of graft-versus-host disease. *Blood.* 122:2251–2261. https://doi.org/10.1182/blood-2013-03-492397

Walseng, E., K. Furuta, B. Bosch, K.A. Weih, Y. Matsuki, O. Bakke, S. Ishido, and P.A. Roche. 2010. Ubiquitination regulates MHC class II-peptide complex retention and degradation in dendritic cells. *Proc. Natl. Acad. Sci. USA.* 107:20465–20470. https://doi.org/10.1073/pnas.1010990107

Yamaji, O., T. Nagaishi, T. Totsuka, M. Onizawa, M. Suzuki, N. Tsuge, A. Hasegawa, R. Okamoto, K. Tsuchiya, T. Nakamura, et al. 2012. The development of colitogenic CD4(+) T cells is regulated by IL-7 in collaboration with NK cell function in a murine model of colitis. *J. Immunol.* 188:2524–2536. https://doi.org/10.4049/jimmunol.1100371

Yamazaki, S., M. Patel, A. Harper, A. Bonito, H. Fukuyama, M. Pack, K.V. Tarbell, M. Talmor, J.V. Ravetch, K. Inaba, and R.M. Steinman. 2006. Effective expansion of alloantigen-specific Foxp3+ CD25+ CD4+ regulatory T cells by dendritic cells during the mixed leukocyte reaction. *Proc. Natl. Acad. Sci. USA.* 103:2758–2763. https://doi.org/10.1073/pnas.0510606103

Zimmerman, B., B. Kelly, B.J. McMillan, T.C. Seegar, R.O. Dror, A.C. Kruse, and S.C. Blacklow. 2016. Crystal structure of a full-length human tetraspanin reveals a cholesterol-binding pocket. *Cell.* 167:1041–1051.

Oh et al., https://doi.org/10.1083/jcb.201611141

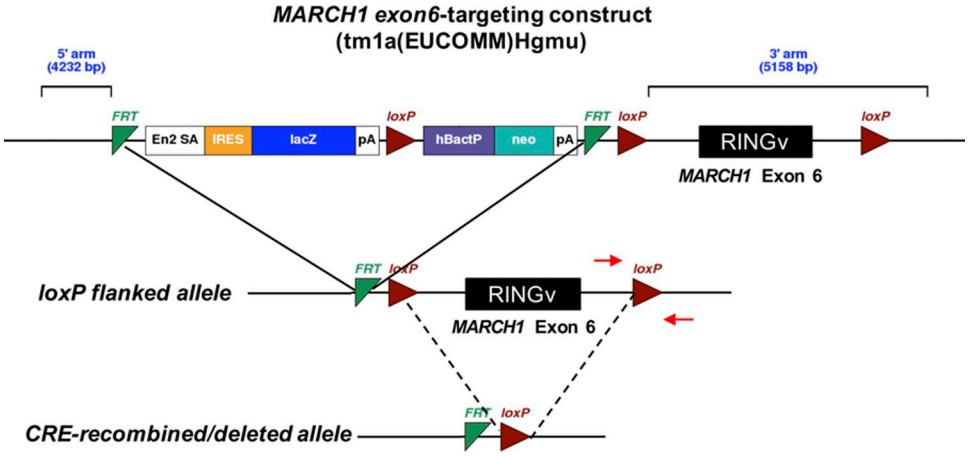

Figure S1. **Generation of MARCH1$^{fl/fl}$ CD11c-CRE mice.** Shown are the maps of the MARCH1 exon6-targeting construct, loxP flanked allele, and CRE recombined/deleted allele. Red arrows indicate the primer pair used to determine the efficiency of Cre-mediated recombination.

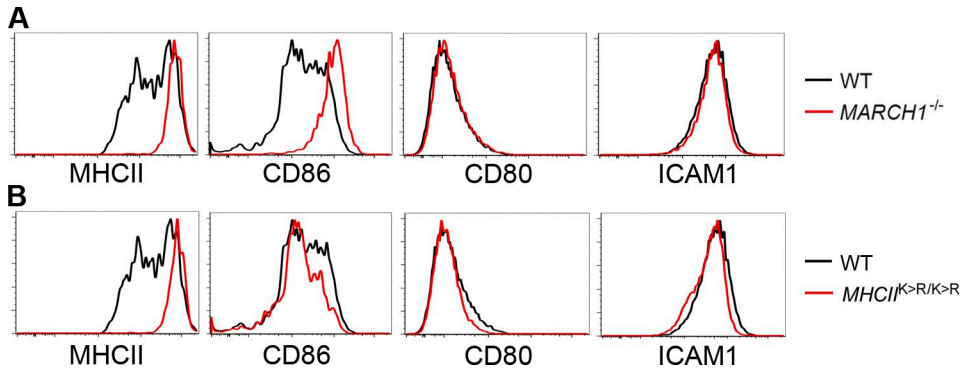

Figure S2. **Surface expression of MHCII, B7 costimulatory molecules, and ICAM1 in thymic DCs. (A)** DCs were isolated from WT or MARCH1$^{-/-}$ mouse thymi and examined by flow cytometry. **(B)** DCs were isolated from WT or MHCII$^{K>R/K>R}$ mouse thymi and examined by flow cytometry. Data represent two independent experiments.

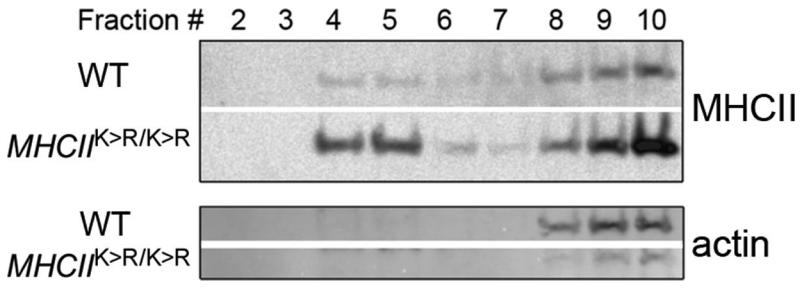

Figure S3. **Association of MHCII with the lipid raft in WT and MHCII K–deficient DCs.** BMDCs derived from WT or MHCII$^{K>R/K>R}$ mice were lysed with 1% Brij58 and fractionated by sucrose density gradient centrifugation as described in our previous study (Shin et al., 2000). Western blot analysis was performed by using antibodies raised against MHCII or actin. Note that some of MHCII molecules were fractionated into the light buoyant-density fractions (#4 and #5).

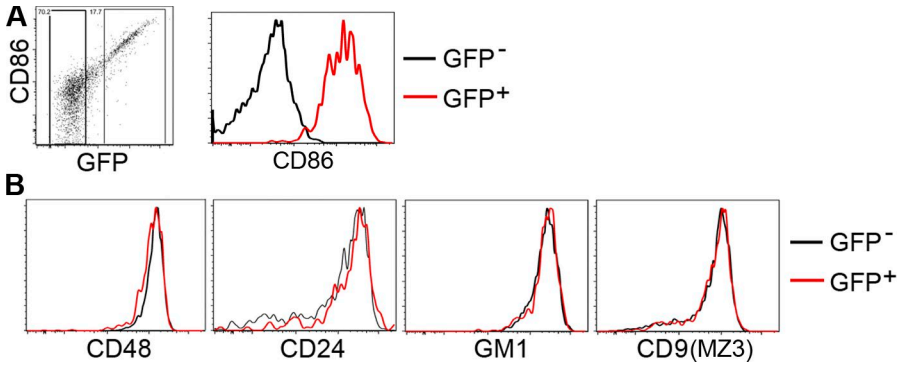

Figure S4. **Excessive accumulation of CD86 in DCs does not alter the lipid raft or tetraspanin web.** BMDCs derived from WT mice were transduced with retrovirus encoding CD86 (K>R) mutant along with cytosolic GFP. The surface level of CD86 in untransduced (GFP^-) and transduced cells (GFP^+) was determined by flow cytometry **(A)**. Cells were stained using antibodies directed against indicated molecules or CTxB (for GM1) and subsequently analyzed by flow cytometry (B).

A

	Genotype of mice	# of mice	Average # of reads per mouse	% of >0.01% filtered TCRs	# of unique TCRs
Treg cells	WT	7	9,735	95.52	181
	MARCH1$^{-/-}$	7	17,217	75.12	80
Non-Treg CD4$^+$ thymocytes	WT	7	11,176	71.64	903
	MARCH1$^{-/-}$	8	15,235	47.25	1559

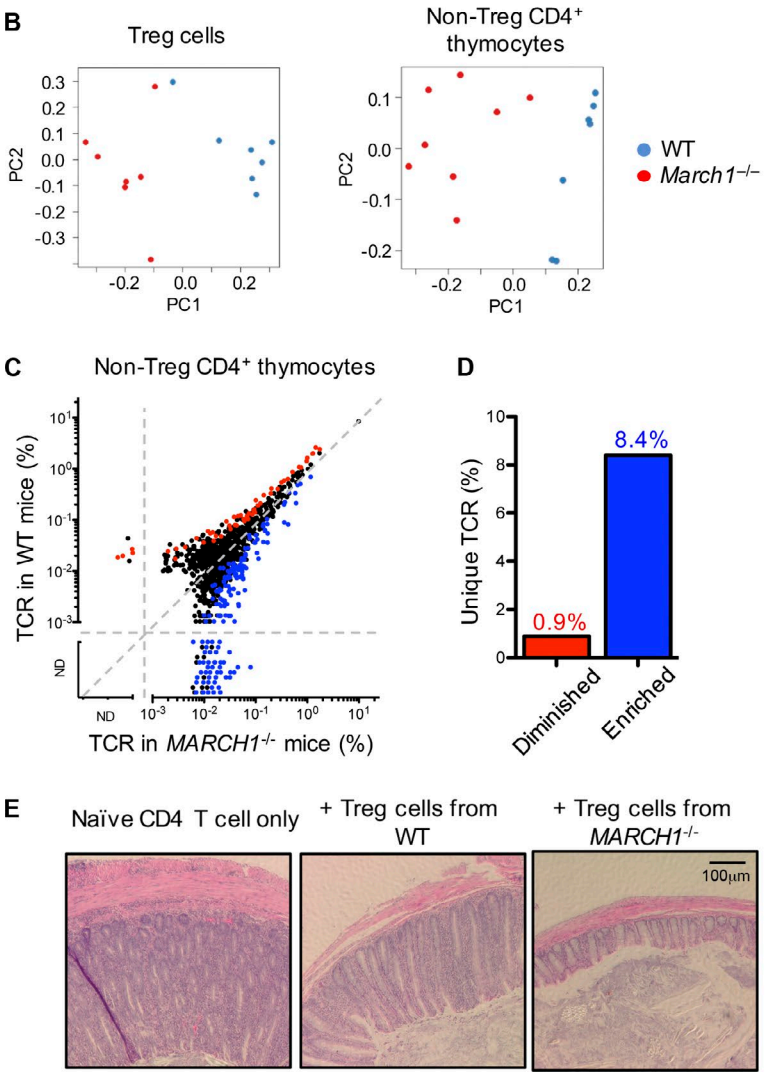

Figure S5. **TCR repertoire analysis and pathology of IBD mouse model. (A)** A table summarizing the TCR repertoire sequencing analysis. ">0.01% filtered TCRs" indicates that the TCR reads present >0.01% in at least one mouse of either genotype. Those TCRs were then further filtered to be characterized as "unique TCRs" if they were present in at least three of seven or eight mice in one genotype. **(B)** Principle component (PC) analysis of sequencing data. Treg cells and non-Treg CD4$^+$ thymocytes are analyzed separately. Each dot represents each mouse. Note that dots are segregated under PC1 by genotype for both Treg cells and non-Treg CD4$^+$ thymocytes. **(C)** Dot plot of unique non-Treg CD4$^+$ thymocyte TCR frequencies in MARCH1$^{-/-}$ versus WT mice. Red and blue dots indicate unique TCRs significantly diminished and enriched in MARCH1$^{-/-}$ mice, respectively ($P < 0.075$, Mann-Whitney U test). ND, not detected. **(D)** The percentages of unique non-Treg CD4$^+$ thymocyte TCR clones diminished or enriched significantly and more than fivefold in MARCH1$^{-/-}$ mice. **(E)** Mice described in Fig. 8 D were euthanized on day 56 after cell transfer, and the distal colons were subjected to histological examination. Representative microscopic images (200×) of hematoxylin and eosin–stained sections are shown.

Reference

Shin, J.S., Z. Gao, and S.N. Abraham. 2000. Involvement of cellular caveolae in bacterial entry into mast cells. *Science.* 289:785–788. https://doi.org/10.1126/science.289.5480.785